LAWRENCE
LIVERMORE
NATIONAL
LABORATORY

LLNL-TR-455813

2010 OFES Joint Research TargetDivertor Heat Flux Profile Width

Final Report

DIII-D Contribution

C. J. Lasnier, M. A. Makowski, J. A. Boedo, D. N. Hill, A. W. Leonard, G. D. Porter, M. E. Rensink, J. G. Watkins

September 17, 2010

Disclaimer

This work performed under the auspices of the U.S. Department of Energy by Lawrence Livermore National Laboratory under Contract DE-AC52-07NA27344.

2010 OFES JOINT RESEARCH TARGET

DIVERTOR HEAT FLUX PROFILE WIDTH

FINAL REPORT

DIII-D CONTRIBUTION

by
C.J. Lasnier, M.A. Makowski, J.A. Boedo, D.N. Hill, A.W. Leonard, G.D. Porter, M.E. Rensink, J.G. Watkins, and DIII-D staff

Work supported by the US Department of Energy under DE-AC52-07NA27344, DE-FG002-07ER4917, DE-FC02-04ER54698, and DE-AC04-94AL85000.

SEPTEMBER 2010

Description of deliverable

Statement of
2010 OFES Joint Research Target

Conduct experiments on major fusion facilities to improve understanding of the heat transport in the tokamak scrape-off layer (SOL) plasma, strengthening the basis for projecting divertor conditions in ITER. In FY10, FES will measure the divertor heat flux profiles and plasma characteristics in the tokamak scrape-off layer in multiple devices to investigate the underlying thermal transport processes. The unique characteristics of C-Mod, DIII-D, and NSTX will enable collection of data over a broad range of SOL and divertor parameters (e.g., collisionality, beta, parallel heat flux, and divertor geometry). Regimes similar to the ITER operating scenarios will be among those studied and characterized. Coordinated experiments using common analysis methods will generate a data set that will be compared with theory and simulation.

DEFINITION OF COMPLETION

Final Report

I. Introduction

Heat flux in a tokamak is transported from the confined core plasma to the edge in a process characterized by the energy confinement time. Energy crossing from the closed field lines to the open field lines at the edge is carried along field lines by ions and electrons while continuing to move outward across field lines due to particle collisions, drifts, and instabilities. Some fraction of the energy is radiated by collisionally excited ions along the way. The open field lines, which form a region called the scrape-off layer (SOL) connect to a limiter or to one or more divertors, where the remaining particle energy is deposited on plasma facing components. Most present and planned tokamaks are designed with divertors, a physical structure combined with a magnetic configuration that gives superior control of impurities. In a divertor the heating of the solid surface is concentrated at the strike points, where the field lines intersect that surface.

The width of the heat flux profile in the divertor $\lambda_{q,div}$ is important to know for the design of future high-power tokamaks. The divertor must be carefully designed to survive the heating by the plasma. To facilitate such designs, we must be able to predict the heat flux by understanding the physics controlling the heat flux profile width on present-day tokamaks, and understand how increases in size, heating power, and plasma temperature will affect that profile in future machines. Prior work studying the parametric dependence of $\lambda_{q,div}$ have arrived at a variety of scalings [1] not all in agreement for JET [2], ASDEX-Upgrade [3], JT60-U [4,5], DIII-D [6,7], and NSTX [8]. The work discussed here is intended to solidify the foundation for the physics understanding of the processes governing $\lambda_{q,div}$.

Experiments were performed in DIII-D both independently and jointly with the National Spherical Torus Experiment (NSTX) at PPPL and the C-Mod experiment at MIT. The CMOD experiments were most closely coordinated since we were able to match more of the relevant plasma parameters between C-Mod and DIII-D than between NSTX and DIII-D. By matching those parameters and examining the differences in the resulting SOL transport, we expect to gain new understanding of those transport mechanisms. The analysis and modeling of this data from the joint experiments is still ongoing and we expect it to be fruitful for some time to come.

The experiments in DIII-D were aimed at both extracting an empirical scaling of the divertor heat flux profile width, and measuring fundamental plasma characteristics to enable detailed numerical modeling of energy transport in the scrape-off layer (SOL). We performed multiple overlapping scans in which plasma parameters were held fixed and some other parameter was varied, including density, toroidal field, plasma current, edge safety factor, and input power. Empirical scaling of the divertor heat flux width has been derived. We found that the heat flux width was dependent mainly upon the plasma current, varying inversely as the 1.24 power of the plasma current. We also obtained edge fluctuation data of the electron density and temperature, to identify the effect of fluctuations on SOL energy transport.

Ultimately the best prediction of the heat flux profile should be obtained by using numerical models that have been shown to contain the appropriate physics by comparing the model with a wide variety of data from existing experiments. Preliminary numerical modeling of the DIII-D discharges has begun, using the UEDGE code.

II. Experiments and data

The initial heat flux experiments discussed here were carried out in 2008. We performed measurements in lower single-null edge localized mode (ELM)ing H-mode diverted configurations. We varied toroidal field (B_T) at constant plasma current (I_p), I_p at constant B_T, and B_T/I_p at constant q_{95}. The neutral beam injected power P_{inj} was changed at constant I_p and B_T. Line-averaged density $\bar{n}_e$ was varied at constant I_p and B_T. The divertor heat flux was calculated from infrared camera measurements using a new high-resolution fast-framing IR camera.

II.A Analysis averaged over ELMs

The initial analysis was carried out by averaging over ELMs. Time windows in the discharges were chosen for nearly constant conditions except for ELMs, and heat flux profiles were averaged over each interval. The full width of the heat flux profile at half-maximum was extracted from each averaged profile and analyzed. The detailed results of this analysis are given in attachment A.

We found essentially no dependence of $\lambda_{q,div}$ on total input power $P_{in}=P_{inj}+P_{Ohmic}$. We illustrate this in Fig. 1, where peak heat flux averaged over ELMs is plotted against input power. The peak heat flux increases linearly with input power. By conservation of energy, the heat flux profile width stays fixed. As found on NSTX, JET and ASDEX-Upgrade (DIVII), we find essentially no (or very weak) dependence of the width on input power.

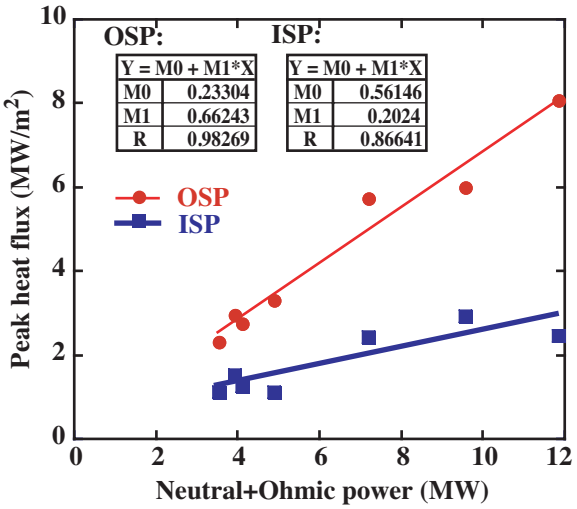

Fig. 1:ELM-averaged peak heat flux at the ISP and OSP plotted against the input power. Linear fits to the data are plotted, with fitting parameters shown in the boxes. The dependence on input power appears linear.

At low density, $\lambda_{q,div}$ was independent of density, up to a threshold signifying the onset of detachment. The effect of radiation from the outboard divertor on the strike point heat flux profile is small for the low-density attached discharges. It becomes significant at the onset of detachment where we see the profile broadening, and in fully detached strike points not considered here, the radiated power absorbed by the divertor plate accounts for nearly all the measured heat flux.

The profile width decreased inversely with increasing plasma current with a very strong correlation (Fig. 2). Density increased with plasma current in these discharges, but remained below the threshold for onset of detachment except at the highest plasma current, where the density was just approaching that threshold. Therefore plots of heat flux profile width versus plasma current are only slightly affected by the density variation.

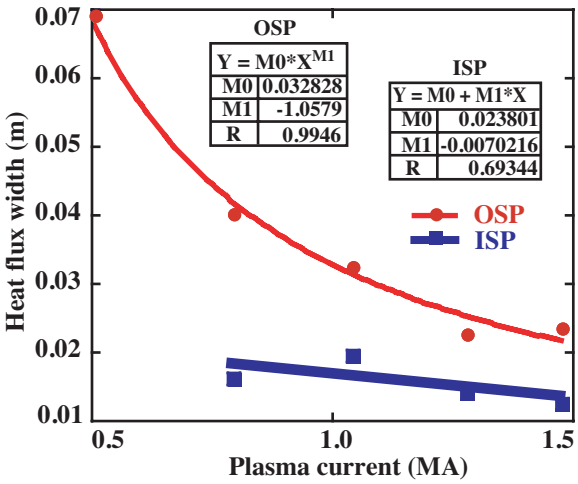

Fig. 2. Widths of profiles, averaged over ELMs, plotted against plasma current. The outer strike point (OSP) shows a clear inverse dependence of width on I_p. The inner strike point (ISP) dependence is less clear, in part because the heat flux is very small at low plasma current.

II.B Inter-ELM analysis

Subsequent analysis was performed by averaging only data falling between ELMS. In this averaging the analysis interval was from 20% to 95% of the relative interval between successive ELMs. Heat flux profiles from these intervals were averaged to form the final result. The heat flux profiles derived in this way were mapped along field lines to the outer midplane by using the magnetic equilibrium reconstruction from the EFIT code.

After the field line mapping, the outside and inside of each profile were fitted with offset exponentials ($a_0 + a_1 e^{x/\lambda}$) as shown in Fig. 3. The heat flux width $\lambda_{q,div,midplane}$ is taken to be the sum of the two exponential widths. In this plot the region to the left of the peak is in the private flux region, so-called because the field lines do not traverse the rest of the poloidal cross-section. The right side is in the SOL. The cause of the offsets from zero heat flux seen in the private flux region and the far SOL are still under investigation. Some heating is known to occur there due to absorption in the surface of radiated power and interaction with very low-density plasma. This heating is calculated to be too small to explain the offset.

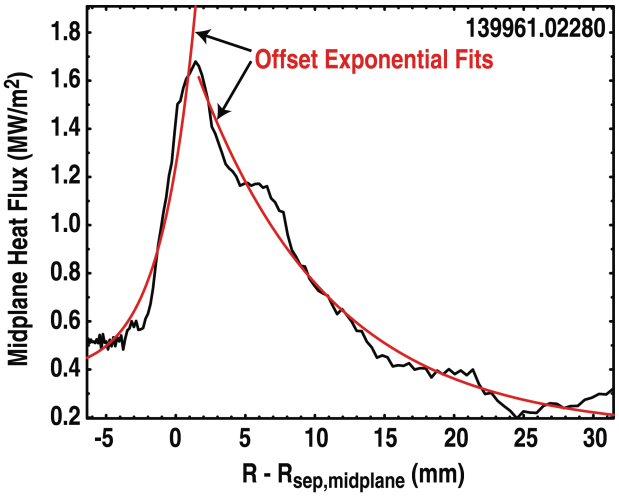

FIG. 3. Typical heat flux profile after mapping to the midplane as a function of distance from the separatrix at the midplane, $R\text{-}R_{sep,mp}$, showing offset exponential fits.

The widths, $\lambda_{q,div,midplane,}$ were used in a multi-parameter fit with independent variables of $B_T, I_p, P_{in}, \bar{n}_e, P_{SOL}$ (the power crossing into the SOL from the main plasma). The detailed results

of this analysis are shown in attachment B. The only significant correlation shown by this fitting process, as seen in Fig. 4, was a dependence of $\lambda_{q,div,midplane}$ on the plasma current:

$$\lambda_{q,div,midplane} = 6.38/ I_p^{1.24} \qquad (1)$$

The blue, black, and red data points of Fig. 4 are taken from different ranges of toroidal field in various discharges, showing no significant effect of changing B_T on $\lambda_{q,div,midplane}$.

We note that the multi-parameter fits also show no trend with B_T. This means that although the connection length is increasing as B_T increases, the transport of energy across field lines is inhibited so that the profile width at the divertor remains nearly unchanged.

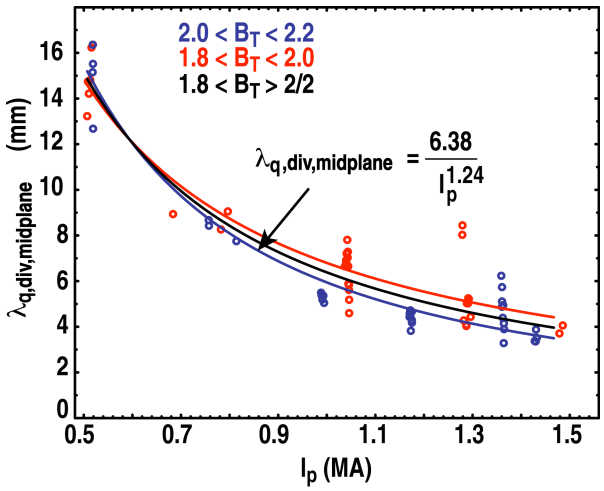

FIG. 4. Dependence of heat flux width (mapped to the midplane) on plasma current. The red, black, and blue symbols denote various ranges of toroidal field, showing little effect from changing B_T.

Equation 1 contains no scaling for machine size because we have not yet compared the DIII-D heat flux data in detail with that from NSTX and CMOD. Therefore it is incorrect to apply equation 1 to a larger machine without modification.

II.B Effect of upstream T_e profile on heat flux profile

Thomson scattering was used to measure upstream temperature and density profiles in the boundary plasma. Magnetic equilibrium reconstructions were once again used to map these profiles to the outer midplane. The profiles just inside and just outside the separatrix were fitted separately with exponential functions. It was found that the SOL-side fits had lower scatter, and it was these that were used in comparisons with $\lambda_{q,div,midplane}$. Electron temperature and density profiles mapped to the outer midplane are shown in Fig. 5, with the respective core-side and SOL-side exponential fits.

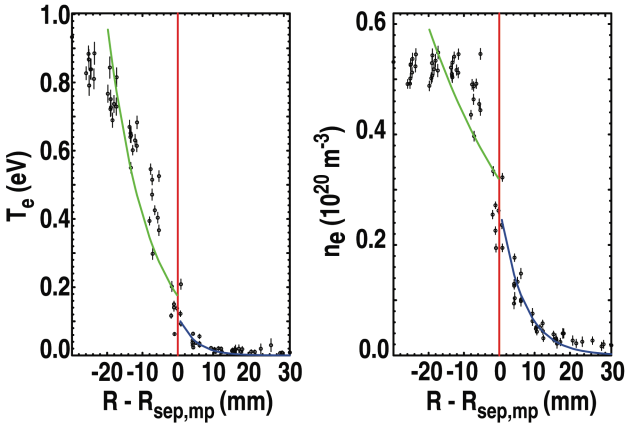

FIG. 5. Typical outer midplane electron temperature and density profiles mapped from Thomson scattering measurements to the outer midplane. The curves show the exponential fits.

In Fig. 6 we show $\lambda_{q,div,midplane}$ plotted against the temperature gradient scale length on the SOL-side of the separatrix, λ_{Te}^{SOL}. The scatter is large and the correlation is weak. This is in contradiction to simple two-point models of SOL transport [9], which would predict that $\lambda_{Te} = (7/2)\,\lambda_q$.

We can conclude that the heat flux profiles for the most part are wider than predicted by the two-point model. Departures from that model are to be expected due to the presence of radial transport, radiation within the transport volume, and recycling in the divertor, which these two-point models neglect.

For discussion of comparisons of the two-point model with UEDGE calculations, see Attachment C. That work also makes clear that the two-point model alone does not adequately describe energy transport in the SOL.

II.C Comparison with other scaling results

The results of the present scaling study are in rough agreement with the JET scaling of conduction limited heat flux widths [10], given by

$$\lambda_{q,\mathrm{miplane}}^{\mathrm{JET}}\ (\mathrm{mm}) = 2.41\times10^{-5}\ B_T^{-1}(\mathrm{T})\ P_{\mathrm{SOL}}^{-1/2}\ (\mathrm{MW})\ n_e^{1/4}\left(\mathrm{m}^{-3}\right) q_{95}R^2\ (\mathrm{m}) \quad . \qquad (2)$$

The dominant dependence is in $q_{95}/B_T \sim 1/I_p$. The density dependence is weak in the JET scaling law, in agreement with our observations. However, our fits show no dependence on P_{SOL}, the power crossing the separatrix. With no machine size variation in our data to compare with the R^2 dependence from JET, we are left with $1/I_p$ from Eq. (2), which is similar to our finding.

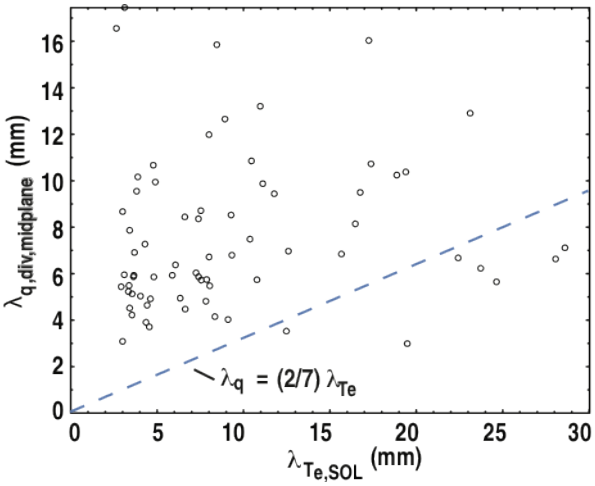

FIG. 6. Plot of the heat flux width, $\lambda_{q,\mathrm{div,midplane}}$, versus the Thomson electron temperature profile e-folding length in the scrape off layer, λ_{Te}^{SOL}. The lengths are larger than expected from a two point model, λ_q= (2/7) λ_{Te}, which is shown by the blue dashed line.

II.D Comparison of Divertor Heat Flux Profiles with UEDGE Modeling

Preliminary modeling of discharges from the plasma current scan shown in Fig. 4 has begun, using the UEDGE code [11]. These results are discussed in detail in Attachment B. The power flow through the SOL, and the midplane electron temperature and density profiles are taken from the experimental data, from a 1.5 MA discharge. Transport coefficients in UEDGE are adjusted until the upstream profiles agree with the experiment. In the results reported here, best agreement with the heat flux width was obtained when drifts were turned on at 20% of full value, and poor agreement when drifts were turned off. The experimentally determined heat flux is much lower than that in the model result, a discrepancy we are working to resolve.

The radiated power in the model (300 kW) also most closely matched the experimentally measured power (350 kW) when the drifts were turned on at 20% of the full value. This shows that drifts are important, but further work is needed to match both the drifts and the measured profile values.

II.E Joint experiment between DIII-D and C-Mod

We performed a set of experiments in DIII-D in a configuration close to one which could be run on C-Mod, and closest to a shape that NSTX could run. We used a shape based on that developed by Groebner , Mossesian , Moyer et al. on Feb. 14, 2001, for "Edge Similarity Experiments on C-Mod and DIII-D". This equilibrium is similar to the ITER shape. C-

Mod later made a shape similar to this, with the same elongation (κ) , triangularity δ (upper and lower), squareness (ξ), and edge safety factor q95. NSTX has data in a shape that matched some shape parameters.

We varied P_{in}, I_p, and B_T stepwise. Each value was held long enough to perform a small strike point sweep for divertor Langmuir probe profile data. The shape was lower single null, with the outer strike point on top of the shelf at R=145-150 cm in order to make it visible to an IR camera viewing it from an R+2 port. We measured both ELM and inter-ELM heat flux. By making comprehensive measurements we will be able to calculate P_{SOL} and use that as a scaling parameter more appropriate than P_{in}. We will also find how the scalings are affected by ELM frequency.

The CMOD discharges are ICRF-heated. To match this as well as we were able, we used ECH heating during the first half of the day. During the second half we used beam heating and no gyrotrons. For ECH shots, the range of toroidal field scanning was limited in order to keep a resonance inside the separatrix. The weakest toroidal field allowed for the gyrotrons-heated discharges was B_T = -1.6 T. This put the resonance off-axis on the inboard side, but we were still able to place the power inside the separatrix with efficient absorption. The strongest field allowed was B_T = -2.1 T, limited by magnet operation.

The lower cryopump provided some pumping of the private flux region, and the upper pumps contributed a small amount of pumping.

The sequence of shots for the scans was patterned on the sequence developed by Phil West for the heat flux scaling experiment on July 23, 2008 in DIII-D.

III. Conclusion

Experiments have been carried out in DIII-D in coordination with experiments at NSTX and C-Mod, measuring the divertor temperature profiles from which were derived divertor heat flux profiles, and plasma characteristics in the respective scrape-off layer of each machine. ITER-like operating regimes are within the covered range of plasma parameters. This data set satisfies the deliverable requirement for this milestone.

This data set will enable detailed study of the mechanisms of heat flux transport in the scrape-off layer that govern the divertor heat flux profile width, and evaluation of modeling codes against data covering a wide range of collisionality, beta, parallel heat flux, and divertor geometry. Data sets are being exchanged between the research staff of the various facilities to enable all to investigate the full range of experimental parameters. Comparison of full 2D numerical models to this data is now in progress. This will result in models adapted to handle this wider range of parameters, and allow more confident and accurate extrapolation of the models to future machines. We have found that a simple two-point model is not adequate to describe transport in the SOL.

DIII-D data has been examined for empirical scaling of divertor heat flux profile widths. We find that the primary dependence is heat flux profile width varying inversely as the 1.24 power of the plasma current. We anticipate improved understanding of the physics responsible

for this effect from numerical modeling now in progress. Ongoing comparisons of data from the three machines will result in additional information about the scaling with machine size. SOL electron temperature and density fluctuations were also measured in DIII-D, so that SOL heat flux transport can be compared with fluctuation levels over the full range of experimental parameters. This will allow benchmarking of codes that calculate fluctuation levels from first principles, and in turn allow us to quantify the effect of these fluctuations on SOL transport.

References

[1] LOARTE, A., *et al.,* Nucl Fusion **47** (2007) S203
[2] EICH, T., *et al.,* J. Nucl. Mater. **333-339** (2005) 669
[3] HERRMANN, A., Plasma Phys. Control. Fusion **44** (2002) 883
[4] ITER Physics Basis Editors, Nucl. Fusion **39** (1999) 2137
[5] LOARTE, A., *et al.,* J. Nucl. Mater. **266-269** (1999) 587
[6] HILL, D.N., *et al.,* J. Nucl. Mater **196-198** (1992) 204
[7] LASNIER, C.J., *et al.,* Nucl. Fusion **38** (1998) 1225
[8] MAINGI, R., *et al.,* J. Nucl. Mater **363-365** (2007) 196
[9] PITCHER, C.S. AND STANGEBY, P.C., Plasma Phys. Control. Fusion **39** (1997) 779
[10] KIRNEV, G., *et al.*, Plasma Phys. Control. Fusion **49** (2007) 689
[11] ROGNLIEN, T., *et al.,* J. Nucl. Mater. **196-198** (1992) 347

LIST OF ATTACHMENTS

A. "Scaling of divertor heat flux profile widths in DIII-D" (Lasnier PSI paper)

B. "Comparison of upstream T_e profiles with downstream heat flux profiles and their implications on parallel heat transport in the SOL in DIII-D" (Makowski PSI paper)

C. "Comparison between 2D simulation and the standard 2-Point model for scrape-off layer transport including effects of spatially varying transport coefficients" (Hill PSI paper)

D. "Scaling of divertor heat flux profile widths in DIII-D" (Lasnier IAEA paper)

Attachment A

Scaling of divertor heat flux profile widths in DIII-D

C.J. Lasnier[a*], M.A. Makowski[a], J.A. Boedo[b], S.L. Allen[a], N.H. Brooks[c], D.N. Hill[a], A.W. Leonard[c], J.G. Watkins[d], and W.P. West[c]

[a]*Lawrence Livermore National Laboratory, Livermore, California 94550, USA*

[b]*University of California-San Diego, San Diego, California 92093, USA*

[c]*General Atomics, P.O. Box 85608, San Diego, California 92186-5608, USA*

[d]*Sandia National Laboratories, Albuquerque, New Mexico 87185, USA*

Abstract

New scalings of the dependence of divertor heat flux peak and profile width, important parameters for the design of future large tokamaks, have been obtained from recent DIII-D experiments. We find the peak heat flux depends linearly on input power, decreases linearly with increasing density, and increases linearly with plasma current. The profile width has a weak dependence on input power, is independent of density up to the onset of detachment, and is inversely proportional to the plasma current. We compare these results with previously published scalings, and present mathematical expressions incorporating these results.

JNM keywords: P0500 Plasma-Materials Interaction, P0600 Plasma Properties

PSI-19 keywords: Cross-Field Transport, DIII-D, Divertor plasma, parallel transport, Power deposition

PACS: 52.25.Fi, 52.40.Hf, 52.55.Fa, 52.55.Rk

**Corresponding and presenting author address: General Atomics, P.O. Box 85608, San Diego, California 92186-5608, USA*

*Corresponding and presenting author e-mail: Lasnier@LLNL.gov

I. Introduction

The width of the divertor heat flux profile $w_{q,div}$ is of great interest in future large tokamaks as well as many present devices. Previous studies examining the parametric dependence of $w_{q,div}$ have arrived at diverse scalings [1] in JET [2], ASDEX-Upgrade [3], JT60-U [4,5], DIII-D [6,7], and NSTX [8] with results somewhat at variance with each other. We attempt here to perform a new series of experiments in DIII-D to obtain scaling of the divertor heat flux peak value, profile width, and divertor plate power as a function of plasma input parameters, with the maximum number of divertor and scrape-off layer (SOL) diagnostics brought to bear.

We performed measurements in lower single-null edge localized mode (ELM) H-mode diverted configurations that, due to the strike-point positions, were not strongly pumped. We varied the plasma current I_p at constant toroidal field B_T, and varied line-averaged density $\bar{n}_e$ at constant I_p and B_T. The neutral beam injected power P_{inj} was varied at constant I_p and B_T, B_T at constant I_p, and B_T/I_p at constant q_{95}. The divertor heat flux was calculated from infrared camera measurements using a new high-resolution fast-framing IR camera.

The IR camera recorded divertor plate surface thermal emission at multi-kilohertz frame rates through the whole discharge to allow measuring time-averaged data as well as rapid changes due to ELMs. The heat flux at each position in the radial profile was calculated at each of the times steps using the THEODOR 2D heat flux analysis code [9]. We show scaling of the divertor peak heat flux and profile width as a function of the parameters varied, and compare with published results from other devices.

II. Peak divertor heat flux

For each discharge, one or more time intervals of interest were selected where plasma conditions varied little during the interval. The average of each quantity was compiled for each interval. Low-frequency ELMs are included in the average.

Figure 1 shows the peak heat flux $q_{div,peak}$ at the inner (ISP) and outer strike points (OSP) plotted against the input power P_{in} (neutral beam heating plus Ohmic heating power), where I_p = 1.3 MA, B_T = -1.9 T were held constant. Density was between 5.2 and 6.5×10^{19} m^{-3}, except at the highest power, where $\bar{n}_e = 2.3\times10^{19}$ m^{-3}. Linear fits are shown. A linear dependence of $q_{div,peak}$ on input power can reasonably be concluded, with the caveat that not all points were taken at the same density. Without the highest power point, we still see a linear dependence.

Figure 2 again shows $q_{div,peak}$ at the ISP and OSP, this time plotted against line-averaged density, where P_{in} = 4.9-5.1 MW except for the densities $\bar{n}_e = 5.2\times10^{19}$ m^{-3}, where P_{in} = 7.2 MW, and $\bar{n}_e = 6.8\times10^{19}$ m^{-3} where P_{in} = 4.1 MW. Toroidal field was held constant at B_T = -1.9 T, and plasma current was held at I_p = 1.3 MA. Linear fits to the data are shown. If the two density values where P_{in} varied are eliminated, the dependence of $q_{div,peak}$ on density still is linear.

Figure 3 depicts the $q_{div,peak}$, now plotted against plasma current, showing a linear dependence. Toroidal field was held at B_T =-1.9 T, and P_{inj} = 4.7–5.0 MW except for the point at I_p = 1.3 MA where P_{inj} = 4.1 MW. Density was not held constant, but allowed to vary at the natural H-mode density, because of practical difficulty measuring the heat flux at the OSP during the plasma pumping that would have been required to maintain constant density. Figure 4 shows

the line-averaged density variation during the I_p scan. Because of the density variation in this set, this plot does not prove the variation with I_p alone. In combination with the density scan at constant I_p, the dependence on I_p will be extracted from a multi-parameter fit to a larger data set in a later analysis.

Figure 5 shows $q_{div,peak}$ plotted against B_T at nearly constant safety factor q_{95} = 3.6-3.7, with linear fits. Density ranged from $\bar{n}_e = 3.2 \times 10^{19}$ m^{-3} at the lowest field to $\bar{n}_e = 5.8 \times 10^{19}$ m^{-3} at the highest field. There are not enough data points to conclusively show a linear dependence, but that would be consistent with the data. Since we know from Fig. 2 that the $q_{div,peak}$ decreases with increasing density, this indicates that if density were held constant, $q_{div,peak}$ would increase faster than linearly with increasing toroidal field magnitude at constant q_{95}.

The work of Makowski [10] indicates that the heat flux profile width does not depend specifically on the toroidal field. If the width does not change the peak cannot change, by conservation of energy. Therefore most likely the dependence of the peak heat flux directly on toroidal field is weak if any, and the dependence shown in Fig. 5 is a result primarily of the I_p variation required for maintaining fixed q_{95}. The fits to $q_{div,peak}$ vs input power in Fig. 1 nearly pass through the origin, which we expect it should since there will be no steady-state heat flux at zero input power. We will assume here that the correct fit should pass through zero. We also know from previous work [7] that the heat flux depends as expected on flux expansion from the outer midplane to the divertor plate. This means the dominant dependence of $q_{div,peak}$ at the outer strike point as found above is expressed by

$$q_{div,peak,out} = aP_{in}\left(9.9 - 9.3n_e\right)\left(-1.5 + 3.9I_p\right)\left(R_{div}B_{div}/R_{mp}B_{mp}\right) \quad , \tag{1}$$

where n_e is the line-averaged density in units of 10^{20} m^{-3}, B_{mp}/B_{div} is the ratio of poloidal magnetic fields at the outer midplane separatrix and divertor, and R_{mp} and R_{div} are the major radii at the outer midplane and divertor respectively. The factor $R_{mp}B_{mp}/R_{div}B_{div}$ gives the flux expansion, I_p is in megamperes, and $q_{div,peak,out}$ is in units of MW/m^2. For the inner strike point,

$$q_{div,peak,in} = bP_{in}\left(3.8 - 3.7n_e\right)\left(-0.7 + 1.5I_p\right)\left(R_{div}B_{div}/R_{mp}B_{mp}\right) \quad . \tag{2}$$

For the discharges used here, the flux expansion at the outer strike point was 6.7 and at the inner strike point, 3.1 (again referenced to the outer midplane separatrix). By plotting $q_{div,peak,outer}$ vs the [right hand side of (1)] $/a$ and drawing a line through the data and the origin, we find $a = 0.006 \pm 0.001$ and an analogous procedure for equation (2) gives $b = 0.05 \pm 0.008$. Other fitting parameters in equations (1-4) have a comparable fractional margin of error. The parameters a and b include some geometry dependence such as scaling with size of the tokamak, which is constant within this data set.

III. Divertor heat flux profile width

Profile widths discussed here are full width at half maximum (FWHM) values for the ISP and OSP respectively. Widths are obtained at each time point and averaged over the time intervals of interest. Here $w_{q,div}$ shows no dependence on P_{in} (not shown). This is consistent with $q_{div,peak}$ varying linearly with P_{in} in the sense that energy is conserved when P_{in} changes.

Figure 6 shows the outer and inner $w_{q,div}$ plotted against density, for the same density scan

as above. There is no effect at low density, but there is a threshold density where the profile becomes wider. Radiated power increases at higher density, but not enough to account for the decreased peak heat flux at the measured widths. It is likely that some energy is deposited in locations that are not measured.

In Fig. 7 is seen $w_{q,div}$ plotted against I_p, for the current scan already described. We see that widths become larger at low current. The fitted curve for the ISP is linear, but for the OSP, a better fit goes inversely as nearly the first power of the plasma current. No ISP heat flux peak was seen at the lowest I_p. We expect the current dependence of the inner width would be of a similar functional form to that of the OSP if more data were available. In Fig. 3, the peak heat flux for this case at the ISP is very small. The dependence $w_{q,div} \propto 1/I_p$ at least at the OSP from Fig. 7 is consistent with $q_{div,peak} \propto I_p$ from Fig. 3 so that total power is preserved when I_p varies.

Because the density scan was performed at constant I_p, we know the effect of density on the heat flux profile width independent of I_p. Fig. 6 shows that the effect of density on $w_{q,div}$ is very weak below the detachment threshold. As shown in Fig. 4, the I_p scan was performed at densities below this threshold so that density dependence does not enter significantly in the I_p dependence depicted in Fig. 7.

The plot in Fig. 8 shows $w_{q,div}$ versus toroidal field at constant q_{95} for the same discharges as described for the peak heat flux scaling. The widths decrease linearly with the magnitude of the toroidal field. This decrease in $w_{q,div}$ is consistent with the increase in $q_{div,peak}$ with increasing magnitude of toroidal field at constant q_{95}.

As with the discussion of Fig. 5, we know form the work of Makowski [10] that the width

does not depend specifically on the toroidal field, and therefore the variation seen in Fig. 8 results primarily from the I_p variation required for maintaining fixed q_{95}. The dependence of the width on power and density are weak (for densities below the detachment threshold). Again taking into account the flux expansion, the dominant $w_{q,div}$ scaling from Fig. 7 for the outer divertor heat flux can be expressed as

$$w_{q,div,out} = 0.0049\left(R_{mp}B_{mp}/R_{mp}B_{div}\right)/I_p^{1.06} \quad , \tag{3}$$

where, I_p is in megamperes, and $w_{q,div,out}$ is in meters. The very small range of variation of inner strike point width in this data set does not yield a useful scaling.

IV. Comparisons with other empirical scalings

Loarte summarized several empirical scalings in Ref. 1, pointing out the areas of disagreement. Here we compare the functional dependences seen above with those scalings.

The linear dependence of $q_{div,peak}$ on power seen above is in agreement with the JET, ASDEX-Upgrade (DIVIII), and previous DIII-D scaling, but not the ASDEX-U (DIVI) scaling. We note that several of those studies use divertor or target power rather than input power. We find the same linear correlation of peak heat flux with target power as with input power.

We have not observed a clear dependence of peak heat flux on toroidal field at fixed I_p in the present data, unlike the previous DIII-D study which found a variation of $1/B_T^{0.5}$. The linear increase in peak heat flux with I_p peak agrees with the previous DIII-D result.

The ASDEX-U scaling found $q_{div,peak}$ varied inversely with density, which we also see.

The $w_{q,div}$ we use here is different than the λ_q of the referenced studies, which defined an effective width by dividing the strike point power by the peak heat flux. We find in agreement

with NSTX, JET IR and ASDEX-Upgrade (DIVII), essentially no (or very weak) dependence of the width on power. We find in agreement with NSTX that the width decreases with increasing plasma current, approximately as $1/I_p$.

V. Conclusion

In the present study we find that peak heat flux varies linearly with input power, inversely as density, linearly with plasma current with a caveat that density was not fixed, and linearly with the magnitude of the toroidal field with q_{95} held constant (primarily because of the change in I_p and not B_T).

We find FWHM $w_{q,div}$ depends not at all on power, and not on density at low density. There is a density threshold for profile broadening associated with the onset of detachment. We see $w_{q,div}$ varies inversely with the I_p and decreases linearly with increasing B_T at constant q_{95}.

We expect to examine this data set further with other fitting techniques as well as making a study of the ELM heat flux profiles from the parameter scans above.

Acknowledgment

This work was supported by the U.S. Department of Energy under DE-AC52-07NA27344, DE-FG02-07ER54917, DE-FC02-04ER54698, and DE-AC04-94AL85000.

References

[1] A. Loarte, *et al*., Nucl Fusion **47** (2007) S203.

[2] T. Eich, *et al*., J. Nucl. Mater. **333–33**9 (2005) 669.

[3] A. Herrmann, Plasma Phys. Control. Fusion **44** (2002) 883.

[4] ITER Physics Basis Editors, Nucl. Fusion **39** (1999) 2137.

[5] A. Loarte, *et al*., J. Nucl. Mater. **266–269** (1999) 587.

[6] D.N. Hill, *et al*., J. Nucl. Mater. **196–198** (1992) 204.

[7] C.J. Lasnier, *et al*., Nucl. Fusion **38** (1998) 1225.

[8] R. Maingi, *et al*., J. Nucl. Mater. **363–365** (2007) 196.

[9] A. Herrmann, *et al*., Plasma Phys. Control. Fusion **37** (1995) 17.

[10] M.A. Makowski, *et al*., "Comparison of upstream T_e profiles with downstream heat flux profiles and their implications on parallel heat transport in the SOL in DIII-D," these proceedings.

Figure Captions

Fig. 1: Peak heat flux at the ISP and OSP plotted against the input power. Linear fits to the data are plotted, with fitting parameters shown in the boxes. The dependence on input power appears to be linear.

Fig. 2: Peak heat flux at the ISP and OSP plotted against line-averaged density. As density increases, $q_{div,peak}$ decreases linearly.

Fig. 3: Peak heat fluxes, now plotted vs I_p. As I_p increases, $q_{div,peak}$ increases linearly.

Fig. 4: Line-averaged density variation during the I_p scan. All the densities are below the detachment threshold.

Fig. 5: Peak heat fluxes plotted against B_T at constant q_{95}, showing a reasonable fits to a line. The heat flux variation is primarily due to the change in I_p and not B_T.

Fig. 6: OSP and ISP heat flux profile widths plotted against density. Density variations below the detachment threshold have no effect on the width.

Fig. 7: Profile widths plotted against plasma current. The OSP shows a clear inverse dependence of width on I_p. The inner strike point dependence is less clear, in part because the heat flux is very small at low plasma current.

Fig. 8: Profile widths versus toroidal field at constant q_{95}. The trend is described by linear fits. The width variation is primarily due to the change in I_p and not B_T.

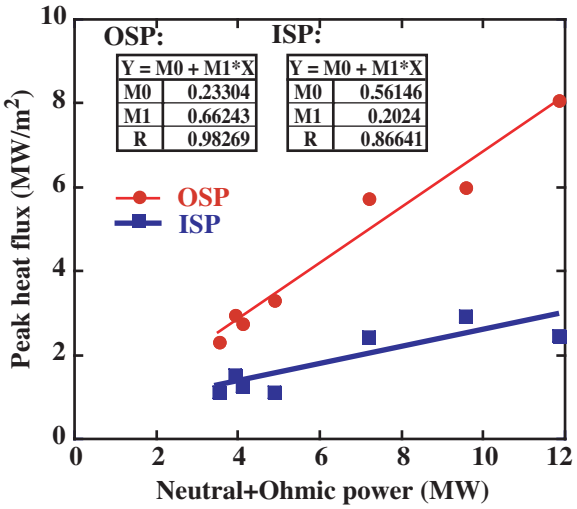
OSP:
ISP:
Y = M0 + M1*X
M0 0.23304
M1 0.66243
R 0.98269
Y = M0 + M1*X
M0 0.56146
M1 0.2024
R 0.86641
OSP
ISP
Peak heat flux (MW/m2)
Neutral+Ohmic power (MW)
0
2
4
6
8
10
12

Figure 1

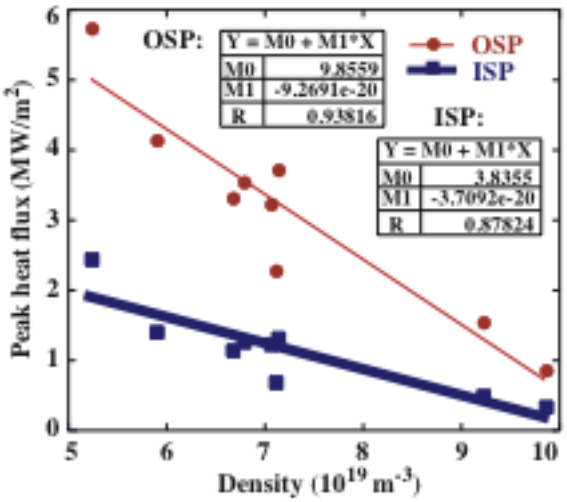
OSP:
Y = M0 + M1*X
M0 9.8559
M1 -9.2691e-20
R 0.93816
OSP
ISP
ISP:
Y = M0 + M1*X
M0 3.8355
M1 -3.7092e-20
R 0.87824
Peak heat flux (MW/m^2)
Density (10^{19} m^{-3})
0
1
2
3
4
5
6
5
6
7
8
9
10

Figure 2

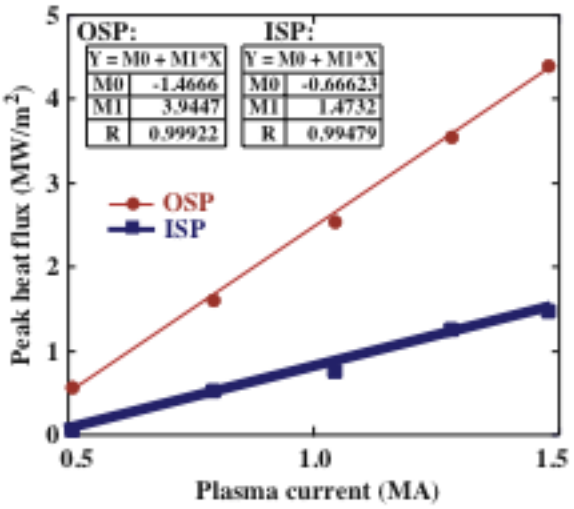
OSP:
Y = M0 + M1*X
M0 -1.4666
M1 3.9447
R 0.99922
ISP:
Y = M0 + M1*X
M0 -0.66623
M1 1.4732
R 0.99479
OSP
ISP
Peak heat flux (MW/m2)
Plasma current (MA)
0
1
2
3
4
5
0.5
1.0
1.5

Figure 3

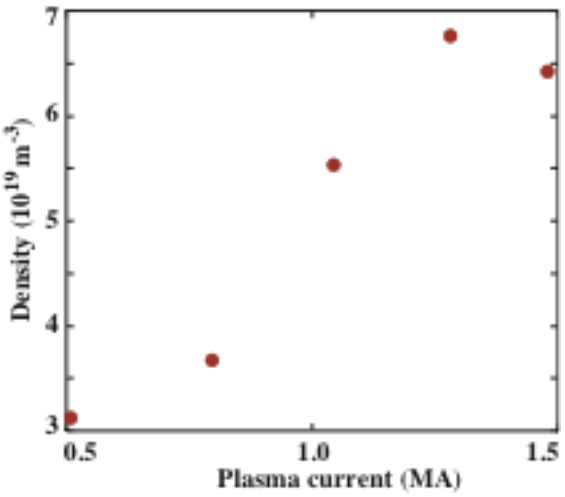

Figure 4

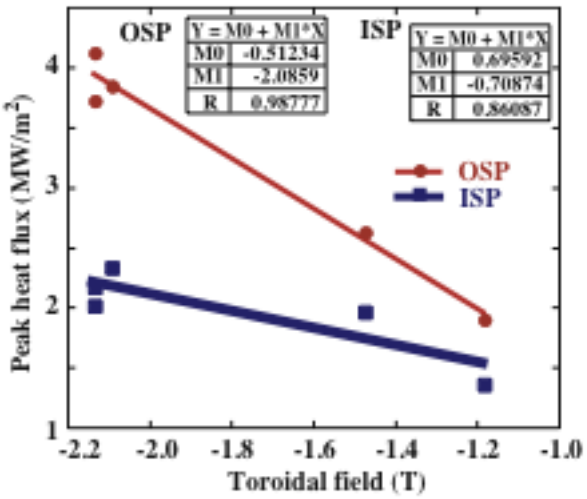
OSP
Y = M0 + M1*X
M0 -0.51234
M1 -2.0859
R 0.98777
ISP
Y = M0 + M1*X
M0 0.69592
M1 -0.70874
R 0.86087
OSP
ISP
Peak heat flux (MW/m²)
Toroidal field (T)
4
3
2
1
-2.2
-2.0
-1.8
-1.6
-1.4
-1.2
-1.0

Figure 5

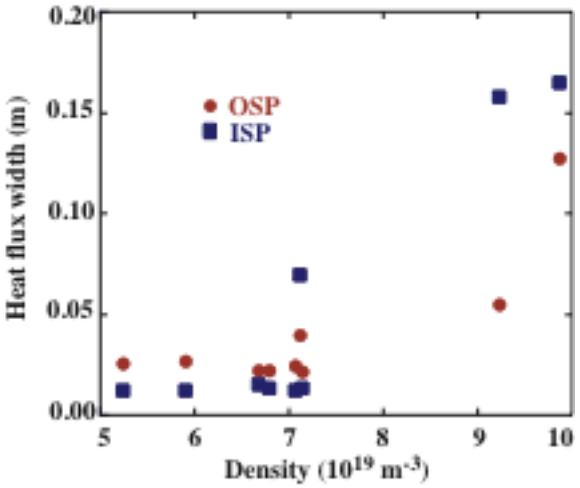
0.20
0.15
0.10
0.05
0.00
Heat flux width (m)
OSP
ISP
5
6
7
8
9
10
Density (10^{19} m^{-3})

Figure 6

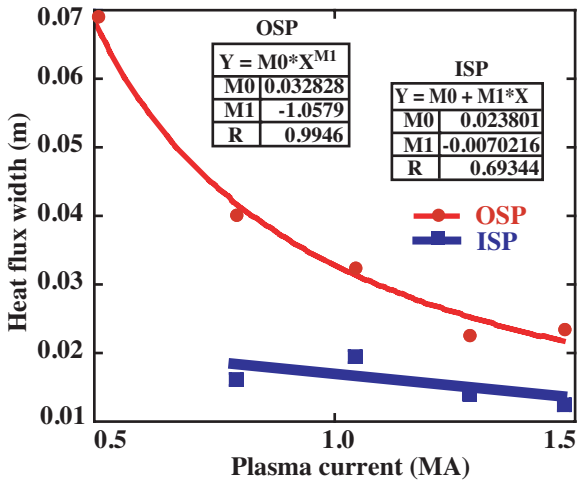
OSP
Y = M0*X^M1
M0 0.032828
M1 -1.0579
R 0.9946
ISP
Y = M0 + M1*X
M0 0.023801
M1 -0.0070216
R 0.69344
OSP
ISP
Heat flux width (m)
0.07
0.06
0.05
0.04
0.03
0.02
0.01
0.5
1.0
1.5
Plasma current (MA)

Figure 7

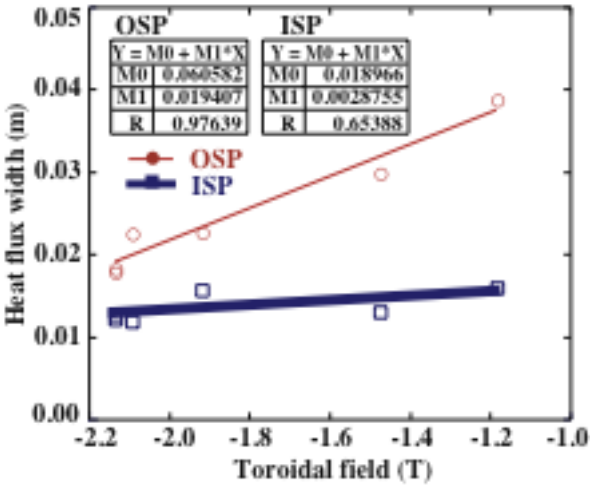
OSP
Y = M0 + M1*X
M0 0.060582
M1 0.019407
R 0.97639
ISP
Y = M0 + M1*X
M0 0.018966
M1 0.0028755
R 0.65388
OSP
ISP
Heat flux width (m)
0.05
0.04
0.03
0.02
0.01
0.00
-2.2
-2.0
-1.8
-1.6
-1.4
-1.2
-1.0
Toroidal field (T)

Figure 8

Attachment B

Comparison of upstream T_e profiles with downstream heat flux profiles and their implications on parallel heat transport in the SOL in DIII-D

M.A. Makowski[a*], C.J. Lasnier[a], A.W. Leonard[b], J. Boedo[c], J.G. Watkins[d], and D.N. Hill[a]

[a]*Lawrence Livermore National Laboratory, Livermore, California 94550, USA*

[b]*General Atomics, P.O. Box 85608, San Diego, California 92186-5608, USA*

[c]*University of California-San Diego, La Jolla, California 92093, USA*

[d]*Sandia National Laboratories, Albuquerque, New Mexico 87185, USA*

Abstract

In DIII-D, we measure the downstream target plate heat flux with an IRTV camera and relate it to Thomson and Langmuir probe profile measurements of n_e and T_e in the scrape-off layer (SOL) by projecting all measurements to the out-board midplane in order to assess the competition between parallel and cross-field heat transport. We analyze the measured characteristic widths associated with the SOL and model the results with the UEDGE code to provide insight into the mechanisms defining the various widths and the implications they have on transport.

Analysis of the scaling of the heat flux width reveals an essentially inverse dependence on I_p. The B_t dependence is extremely weak to non-existent. No dependence was found on the shear and normalized pressure gradient at the 95% flux surface (s_{95}, α_{95}), nor on P_{sol}, n_e or P_{inj}.

JNM keywords: P0500, P0600

PSI-19 keywords: DIII-D, Divertor, Edge modelling, Power Deposition, UEDGE

PACS: 52.40.Hf, 52.55.Rk, 52.55.Fa

**Corresponding and presenting author address: General Atomics, P.O. Box 85608, MS 13-153, San Diego, California 92186-5608, USA*

**Corresponding and presenting author e-mail:* makowski1@llnl.gov

I. Introduction

Experiments were carried out in H-mode plasmas to measure the heat flux width, λ_q, as a function of various plasma parameters including magnetic field, B_t, plasma density, n_e, and injected power, P_{inj}. The heat flux was inferred by using an IRTV camera to measure the temperature that was then converted to a heat flux with the THEODOR code. Care was taken to reduce the influence of ELMs through the use of ELM synchronization, a method of conditionally averaging results between ELM spikes over many ELM cycles. Heat flux and upstream Thomson temperature and density profiles were all analyzed in this fashion.

Using this method, we have extracted gradient scale lengths of electron density and temperature at the midplane, and divertor heat flux widths. These, in turn, have been used to derive scaling relations and to examine parametric dependencies such as the relation of the heat flux width to the upstream electron temperature gradient scale length.

We have also started to model the experimental results with the UEDGE [1] code in an effort to understand the relative importance of cross-field and parallel transport.

II. Upstream Profiles

Upstream, ELM synchronized, edge profiles of n_e and T_e were measured with the Thomson scattering system, located at the upper outer region of the plasma at a major radius of 1.94 m. The profile typically consisted of 5-10 measurements within the 200 ms analysis window. The Thomson data was then mapped to the outer midplane. Simple exponential fits to the data immediately inside and outside the separatrix were made to obtain a measurement of the electron temperature gradient scale length, λ_{T_e}, which was then correlated with the heat flux width. Figure 1 shows typical profiles and exponential fits to both the core- and SOL-side data. It can be

seen that the core-side exponential fit is influenced by the top of the pedestal. Scrape-off layer (SOL) widths from tanh-fits [2] were also considered in the analysis. The trends reported below are independent of which parameter was used as the gradient scale length. To be consistent with other published data, the exponential fit to the SOL-side width has been used in the following.

III. Heat flux results

Heat flux to the lower divertor was measured with an IRTV camera mounted on the top of the vessel. Typically, a set of ~ 300 profiles were averaged to form a single heat flux profile. To facilitate comparison of the various profiles, they have all been mapped to the outer midplane.

These data were used to create a database by dividing each shot into segments 200 ms in length. Each of the plasma parameters was averaged over this interval. ELM synchronization was used to eliminate their influence on the measurements. Additional parameters were also computed such as the shear and normalized pressure gradient at the 95% flux surface $\left(s_{95},\, \alpha_{95}\right)$. Other parameters were included in the database to select good segments, since not all shot segments contained usable data.

Figure 2 shows a typical outer divertor heat flux profile as measured with the IRTV camera for I_p = 0.52 MA. The THEODOR code [3] was used to convert the temperature measured by the IRTV camera to a heat flux. For the profile shown, the THEODOR calculation was performed without including the effect of thermal resistance due to surface carbon layers. Also shown are independent offset exponential $\left(a_0 + a_1 e^{x/\lambda}\right)$ fits to both sides of the heat flux profile. This procedure was necessitated since the low and high field sides of the heat flux profile had different baselines, likely resulting from radiative heating of the private flux region. This made the application of the standard definition of the Loarte width [4]

$$\lambda_q^{loarte} = \frac{\int q_{div}(r) 2\pi R dr}{2\pi R_{div} q_{div}^{peak}} \cdot \frac{R_{div} B_\theta^{div}}{R_{mp} B_\theta^{mp}} \quad ,$$

difficult to apply. The heat flux width λ_q was taken as $\lambda_q = \lambda_{left} + \lambda_{right}$ which can be shown to be closely related to the Loarte width.

The measured heat flux width, λ_q, shows a very weak dependence on the upstream T_e-profile regardless which of the inferred gradient scale lengths was used. Figure 3 shows a plot of heat flux width versus the midplane T_e gradient scale length in the SOL. Due to the scatter in the upstream widths, the correlation coefficient is only 0.124 though, implying that the trend itself is weak. The observed trend is in strong disagreement with simple two-point models that predict $\lambda_{T_e} = (7/2)\lambda_q$ [5]. Given that the slope of the fit is almost zero, a slope of 7/2 predicted by the two-point model, appears to be nearly excluded by the data, despite the low correlation coefficient. The observed weak dependence of λ_{T_e} on λ_q is not an unreasonable result since radial transport, SOL radiation, and divertor recycling affect heat flux within flux tubes; effects not taken account of in the models leading to the cited scaling law.

A variety of multi-parameter fits were attempted to establish scaling laws between the heat flux width, λ_q, and I_p, q_{95}, n_e, B_t, P_{sol}, P_{inj}, s_{95}, and α_{95}. The only significant dependence found was on I_p. The dependence of λ_q is nearly inverse, scaling as $I_p^{-1.24}$ as shown in Fig. 4. The B_t scaling previously reported [6] was not observed in this data. This may be due to the fact that the influence of ELMs was eliminated in this data set through the use of inter-ELM averaging. Also, there were only a limited number of low-field data points in the current data set.

IV. Other scaling laws

There are a number of multi-machine scaling laws in existence. Here we consider two. The first is the JET conduction limited scaling relation [7] given by

$$\lambda_q^{JET}(\text{mm}) = 2.41\times10^{-5} B_T^{-1}(\text{T}) P_{SOL}^{-1/2}(\text{MW}) n_e^{1/4}\left(\text{m}^{-3}\right) q_{95} R^2(\text{m}) \quad .$$

This is in quite good agreement with data from the DIII-D experiment. Figure 5 shows a plot of λ_q^{DIII-D} versus λ_q^{JET}. The bulk of the dependence results from the variation in $q_{95}/B_t \sim 1/I_p$. The result is somewhat fortuitous in that the factor $n_e^{1/4}$ has little influence on the scaling law and no dependence on n_e has been found in our data. The $n_e^{1/4}$ scaling on density is quite weak at any rate. Further, we also observe no dependence on P_{sol} (defined as the total input power, less $\dot{W}$, less the core radiated power), though the scaling law has a $P_{sol}^{-1/2}$ dependence. Since R is a constant for our data, the scaling law reduces to $\lambda_q^{JET} \sim B_t^{-1} q_{95} \sim 1/I_p$, which is essentially the scaling shown in Fig. 4.

We have also considered the multi-machine scaling law from reference [4]:

$$\lambda_q^{H-2}(\text{mm}) = 5.3 P^{0.38}(\text{MW}) B_T^{-0.71}(\text{T}) q_{95}^{0.30} \quad .$$

This is in extremely poor agreement with the DIII-D data and predicts profile widths a factor of 10 lower than those measured in DIII-D. There is no size dependence and the dependence on q_{95} is rather weak.

V. UEDGE simulations

Efforts are underway to model four representative points on the I_p scan of Fig. 4 with UEDGE [1] in order to determine what underlying physics might be changing with I_p to affect

λ_q. Inputs to UEDGE are the power flux through the SOL and the midplane electron temperature and density profiles. Transport coefficients are adjusted within UEDGE to obtain a match between the upstream experimental Thomson profiles and UEDGE profiles and held fixed thereafter. Results are preliminary but still offer some insight. The results reported below are with the flows partially turned on (20% of their full value). Figure 6 shows a comparison of the measured heat flux profile and that obtained from a UDEGE simulation as a function of distance along the target plate for $I_p = 1.5$ MA. The measured profile is scaled by a factor of 5.2 and is thus much lower than that predicted by UEDGE.

With the drifts turned off only ~ 90 kW of power is radiated in the divertor, which is much less than the experimentally measured value of 350 kW. This is caused by a very high value of electron temperature and low value of electron density at the target plate. The high temperature also leads to a large radial electric field that in turn leads to a strong $\mathbf{E} \times \mathbf{B}$ poloidal flow. The flow, in turn, increases n_e at the plate with a corresponding increase in radiated power. With the flows at 30% of their full value (controlled by a parameter in UEDGE) better agreement in the power balance is obtained with ~ 300 kW of radiated power predicted by UEDGE in this case. The UEDGE heat flux profile width is about 25% narrower than the measurement without the flows turned on. With the flows partially turned on, the heat flux profile broadens, but is still narrower than the experimental profile. Note that a shoulder is developing on the right hand side corresponding to the shoulder in the experimental data. No in/out asymmetry of the baseline is present on the UEDGE profile in contrast to the measurement.

VI. Summary

We have measured upstream electron temperature and density profiles and derived gradient scale lengths from them. These have been related to the measured downstream heat flux widths

and a very weak dependence between them has been found between the two quantities. The dependence is much weaker than simple two-point models would predict. A scaling law for the DIII-D heat flux width has been developed and is only dependent on $I_p^{-1.24}$. This is in very good agreement with JET scaling law that takes size into account. UEDGE runs are currently in progress and beginning to yield some insight into the mechanisms influencing the heat flux width. It is already clear that the plasma flows play a significant role in the shaping of the heat flux profile.

Acknowledgment

This work was supported by the U.S. Department of Energy under DE-AC52-07NA27344, DE-FC02-04ER54698, DE-FG02-07ER54917, and DE-AC04-94AL85000. Thanks goes to Gary Porter for his time and patience helping with the UEDGE simulations.

References

[1] T. Rognlien, *et al.,* J. Nucl. Mater. **196-198** (1992) 347-351.

[2] G.D. Porter, *et al*., Phys. Plasmas **5** (1998) 1410.

[3] A. Hermann, *et al*., Plasma Phys. Control. Fusion **37** (1995) 17.

[4] A. Loarte, *et al.,* J. Nucl. Mater. **266-269** (1999) 587-592.

[5] C.S. Pitcher and P.C. Stangeby, Plasma Phys. Control. Fusion **39** (1997) 779.

[6] C. Lasnier, *et al.,* in Proc. 36th EPS Conf. on Plasma Physics, Sofia, Bulgaria, June 29 - July 3, 2009 ECA Vol.33E, P-4.140 (2009).

[7] G. Kirnev, *et al*., Plasma Phys. Control. Fusion **49** (2007) 689.

Figure Caption

Fig. 1. Upstream T_e and n_e profiles mapped to the outer midplane. Fits to exponentials on both the core and SOL sides of the profile are shown. The SOL side fit was used as a measure of the upstream profile gradient scale length.

Fig. 2. Typical heat flux profile as a function of major radius relative to the location of the separatrix at the midplane, $R - R_{sep,mp}$. Also shown in red are offset exponential fits to both sides of the profile.

Fig. 3. Plot of the heat flux width, λ_q, versus the Thomson profile e-folding length in the scrape off layer, $\lambda_{Te,sol}$. Solid red line is a linear fit between the two parameters. The slope, s, is 1/10th that predicted by simple two-point models.

Fig. 4. Plot of the heat flux width, λ_q, versus I_p for two ranges of B_t (red and blue curve fits). Due to the weak dependence of λ_q on B_t, the two curves nearly overlap. The black line is fit to all the data (red and blue circles).

Fig. 5. Plot of $\lambda_q^{DIII=D}$ versus λ_q^{JET} showing that the DIII-D fits the JET scaling law.

Fig. 6. Comparison of measured heat flux (blue, multiplied by 5.2) and that predicted by UEDGE (red). For this case I_p = 1.5 MA.

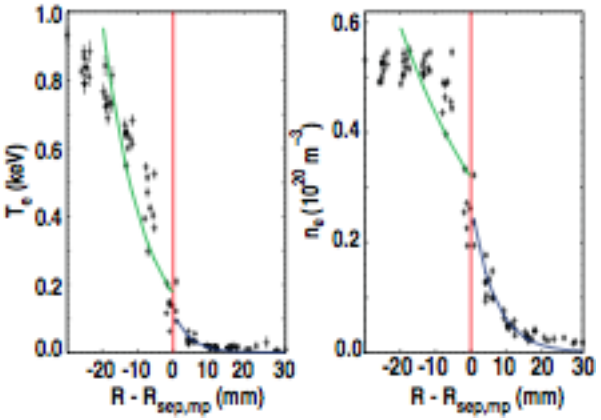
1.0
0.8
0.6
0.4
0.2
0.0
T_e (keV)
-20 -10 0 10 20 30
R - $R_{sep,mp}$ (mm)
0.6
0.4
0.2
0.0
n_e (10^{20} m^{-3})
-20 -10 0 10 20 30
R - $R_{sep,mp}$ (mm)

Figure 1

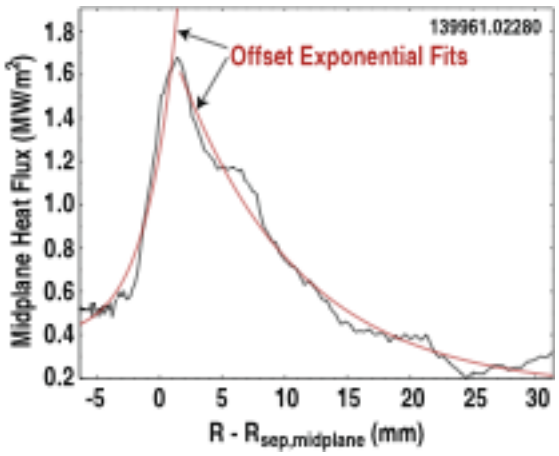
139961.02280
Offset Exponential Fits
Midplane Heat Flux (MW/m²)
1.8
1.6
1.4
1.2
1.0
0.8
0.6
0.4
0.2
-5
0
5
10
15
20
25
30
R - R sep,midplane (mm)

Figure 2

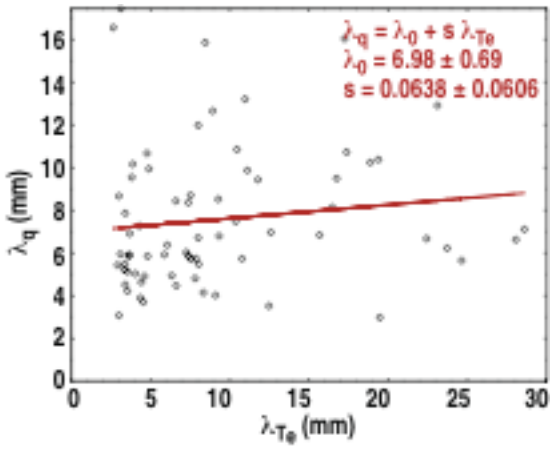
$\lambda_q = \lambda_0 + s\,\lambda_{Te}$
$\lambda_0 = 6.98 \pm 0.69$
$s = 0.0638 \pm 0.0606$
λ_q (mm)
λ_{Te} (mm)
0
2
4
6
8
10
12
14
16
0
5
10
15
20
25
30

Figure 3

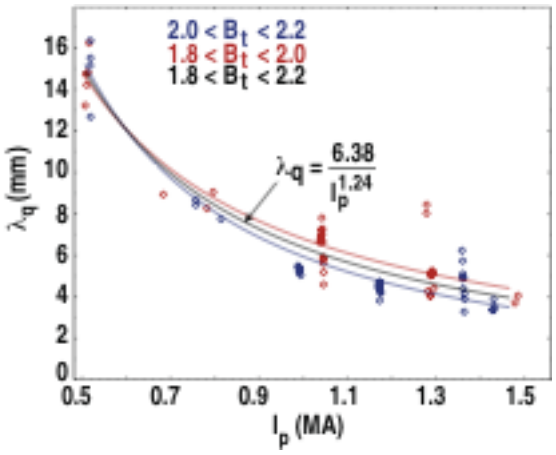
2.0 < Bt < 2.2
1.8 < Bt < 2.0
1.8 < Bt < 2.2
λq = 6.38 / Ip^1.24
λq (mm)
Ip (MA)
0
2
4
6
8
10
12
14
16
0.5
0.7
0.9
1.1
1.3
1.5

Figure 4

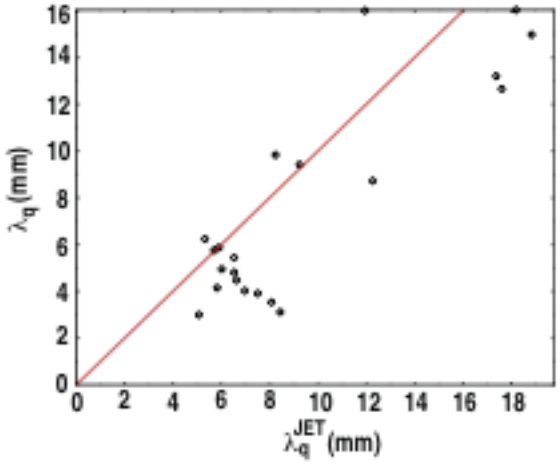

Figure 5

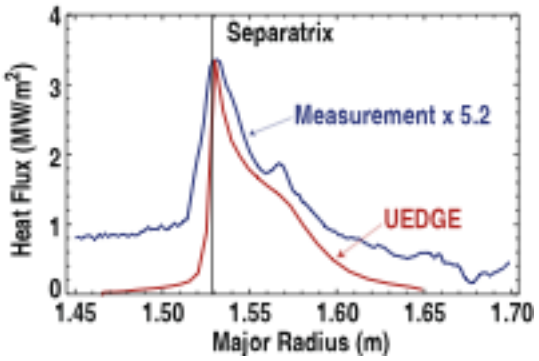
Separatrix
Measurement x 5.2
UEDGE
Heat Flux (MW/m²)
Major Radius (m)
0
1
2
3
4
1.45
1.50
1.55
1.60
1.65
1.70

Figure 6

Attachment C

Comparison between 2D simulation and the standard 2-Point model for scrape-off layer transport including effects of spatially varying transport coefficients

D.N. Hill[a*], G.D. Porter[a], and T.D. Rognlien[a]

[a]*Lawrence Livermore National Laboratory, Livermore, 94550, USA*

Abstract

The effect of 2D transport in the tokamak scrape-off layer (SOL) on relating measured divertor heat flux profiles to midplane plasma profiles is explored with the UEDGE code for a range of transport assumptions. The relationship between the divertor heat flux profile and the midplane plasma temperature profile as determined from UEDGE is compared to commonly used predictions from 1D and "2-point" analytic relation. Results show that the parametric variation in $\lambda_{q,div}$ with midplane separatrix values follows the conduction-limited 2-point model, though the actual valuate of $q_{//}$ on a given flux surface is much lower than implied by the midplane $T_{e,sep}$, and $\lambda_{q,div}$ is ~ twice as wide as expected from these models. Poloidal variations in χ result in minimal change to radial profiles and probably can't be distinguished experimentally from cases with uniform χ having the same flux-surface average value.

JNM keywords: T0100 Theory and modeling, P0500 Plasma-material interaction

PSI-19 keywords: Scrape-off layer simulation, UEDGE, DIII-D, heat flux

PACS: 52.55.Rk, 52.55.Fa, 52.40.Hf, 52.25.Fi

**Corresponding and presenting author address: General Atomics, PO Box 85608, San Diego, California 92186-5608, USA*

Corresponding and presenting author e-mail: hilldn@fusion.gat.com

I. Introduction

The prediction of peak steady-state heat loads on divertor surfaces is an important element for the design of next generation tokamak burning plasma fusion experiments. Predictions can be based on extrapolation from existing measurements and/or numerical simulations which incorporate relevant scrape-off layer (SOL) physics. Due to the complexity of simulations which accurately treat the SOL geometry and the broad range of relevant physical effects, trends in experimental data are often compared against simple 1D or 1.5D analytic approximations.

In this paper we use the UEDGE 2D scrape-off layer simulation code [1] to examine how well the simple models reproduce the properties of the SOL plasma as determined by the more complete treatment. At the same time, we examine the scaling of peak divertor heat flux and profile width with upstream parameters such as electron temperature, power, density, toroidal field (connections length) and transport coefficients. The purpose of this activity is not to evaluate the validity of UEDGE in matching experiment as in [2-4], but rather to use it as a tool to understand the effect of the 2D geometry as it impacts the behavior of the SOL for only the simplest of effects; namely, thermal transport in the absence of large radiative losses, high impurity concentrations, strong flows, and transients.

In the following sections we examine several aspects of SOL thermal transport, first summarizing basic transport equations and the assumptions that result from considering parallel thermal transport as "dominant." Then, UEDGE is used to compute basic SOL parameters and the UEDGE output is compared to the simple model. Finally, the effects of the 2D divertor tokamak geometry and of spatially varying transport coefficients are examined.

II. The SOL dominated by parallel thermal conduction

It is well known that the heat conduction along magnetic field lines is much larger than cross-field thermal conduction [5,6]. At $n_{e,mid} = 2\times10^{19}$ m^{-3} and $T_{e,mid} = 100$ eV with $\chi_e = 1$ m^2/s, parallel and perpendicular power densities are 1.0×10^9 and 6.4×10^4 (W/m^2), for 20 m and 0.5 cm gradient scale lengths, respectively. Parallel thermal conductivity is independent of density, but depends strongly on temperature $\left(T^{5/2}\right)$, while perpendicular conductivity depends on the product of density (n) times the anomalous radial thermal diffusivity for ions (electrons), $\chi_{e,i}$. For electrons, the relations are [5]:

$$q_{\parallel}\left(W/\mathrm{m}^2\right) = -2050T_e^{5/2}\frac{dT_e(\mathrm{eV})}{ds(\mathrm{m})} \quad , \tag{1}$$

for $Z = 1$, and

$$q_{\perp,e}\left(W/\mathrm{m}^2\right) = 3200n\left(10^{20}\ \mathrm{m}^{-3}\right)\chi_e\ \left(\mathrm{m}^2/\mathrm{s}\right)\frac{dT_e(\mathrm{eV})}{dy(c\mathrm{m})} \quad , \tag{2}$$

where s is the distance along field lines and y is the distance perpendicular to a flux surface. While the ratio of parallel to perpendicular power density is large, the total plasma surface area on the separatrix is much larger (~25 m^2 in the DIII-D tokamak) than the cross sectional area of the SOL perpendicular to **B** (0.017 m^2), so both components are important on a flux surface.

Frequently, for qualitative scaling purposes, the radial transport on a flux tube is neglected, so the energy balance can be integrated along field lines, giving the well-known relationship between upstream and downstream electron temperatures for plasmas subject to collisional thermal conduction,

$$q_{\parallel} = \left(T_{e,mid}^{7/2} - T_{e,div}^{7/2} \right) \Big/ L_{\parallel} \quad . \tag{3}$$

Given the large exponent, the downstream temperature can be neglected. If this relationship holds on flux surfaces, the ratio of the heat flux to electron temperature scale lengths immediately follows: $\lambda_{q,mid} \propto {}^{2}\!/_{7}\, \lambda_{T,mid}$, with the divertor heat flux related to the midplane heat flux by magnetic flux expansion.

The integrated 1D model can be expanded by including integrated radial energy transport in the entire SOL, thereby finding the overall e-folding width of the SOL at the midplane, $\lambda_{q,mid}$,

$$\lambda_{q,mid} \propto \frac{q_{95}^{4/9} \; n_{e,mid}^{7/9} \; \chi_{\perp}^{7/9}}{P_{SOL}^{7/9}} \quad , \tag{4}$$

where q_{95} is the safety factor at the 95% flux surface. This is the so-called 2-point SOL model, as discussed in Ref. 2. When the parallel heat flux is limited by the sheath at the divertor plate, the divertor temperature is not much lower than the midplane temperature, and a much weaker dependence on density and power results

$$\lambda_{q,mid} \propto \frac{q_{95}^{2/5} \; n_{e,mid}^{1/5} \; \chi_{\perp}^{3/5}}{P_{SOL}^{1/5}} \quad . \tag{5}$$

These relations will now be compared with UEDGE simulations.

III. UEDGE Simulation Methodology

Here we used the UEDGE code to solve the 2D transport equations (continuity, momentum, and energy) for both ions and electrons. Flux limits to ion and electron parallel thermal conductivity were enabled, but neither particle drifts nor impurity transport and radiation were turned on for this study. The calculated heat flux at the divertor targets includes electron and ion

conduction, convection, classical sheath physics, and recombination energy [2]. Electron thermal conduction dominates power to the plates.

The lower single-null 50 × 30 computational mesh (poloidal × radial) was generated from DIII-D MHD equilibria provided by EFIT, and spanned the entire edge plasma from 3 cm inside the separatrix to 1.8 cm outside the separatrix at the plasma midplane. The non-uniform mesh increased the density of cells where steep gradients are expected (near the separatrix and near the divertor plates) and was sufficient to resolve the expected temperature and density gradients, with the radial range extending far enough into the SOL to capture ~ 90% of the power on the targets; doubling the mesh in both dimensions did not significantly change the UEDGE solutions. Boundary conditions for the simulations were set to the measured core density near the top of the pedestal, and power flow into the SOL (P_{beam} – core radiation loss) typical of lower-single-null H-mode discharges (134079 through 134082), divided equally between ions and electrons.

Scans with UEDGE were carried out by varying only the single parameter of interest (i.e., χ_e with χ_i/χ_e held constant) rather than trying to mimic or match how all the midplane parameters vary when one parameter is changed. Once the run was complete, all relevant quantities were available for plotting and analysis, making it a simple matter to determine gradient scale lengths as a function of position in the SOL, which then could be used to evaluate Eqs. (4) and (5). In all, over 50 UEDGE runs were completed, which included scans of power, density, toroidal field, carbon impurity fraction/radiative loss, and radial transport coefficients.

IV. Analysis of power balance on SOL flux surfaces

Power flows into the tokamak SOL through radial transport across the whole plasma separatrix surface, whereas the basic analysis of Section II assumes that power flows into the

SOL at a single poloidal location. As the full 2D UEDGE simulation shows, the immediate consequence is that in the SOL, and so knowing the midplane electron temperature does not directly specify the parallel heat flux on a flux surface. The red curve in Fig. 1 shows that the poloidal distribution of the perpendicular heat flux across the separatrix into the SOL $(q_\perp)$ is strongly peaked at the outboard midplane (defined as $\theta_{pol} = 270°$) due to the radial compression of flux surfaces there, even when the radial transport (χ_e and χ_i) is spatially uniform. Further, the parallel heat flux does not peak at the same place as $q_\perp$, but down near the x-point, closer to the divertor targets, and there is a stagnation point (zero parallel heat flux) near the top of the plasma, opposite the x-point. Yet, as shown, the electron temperature in the SOL remains high around the whole boundary.

Another effect also comes into play which further breaks the relation between downstream heat flux (near the divertor targets) and midplane T_e implied by Eq. (3). Radial transport removes energy from high-temperature flux surfaces near the separatrix to neighboring, cooler flux surfaces further out in the SOL. For example, with $\chi_e = 0.5\ \mathrm{m}^2/\mathrm{sec}$ (a common value derived from fitting T_e profiles in DIII-D H-mode discharges), half the total power crossing the separatrix is transported radially outward completely through the first 2 mm of the SOL closest to the separatrix, leaving only half to arrive at the corresponding location near the strike points on the divertor target. In Fig. 2 we plot the heat flux at the outer divertor target as determined from UEDGE (2D solution) and the heat flux as determined from Eq. (4) using $T_{e,mid}$ from UEDGE vs the radial distance from the separatrix strike point. As shown, on any flux surface across the SOL, the actual divertor heat flux is only about 30% of that implied by the simple 1D analysis and upstream electron temperature. This ratio is fairly independent of χ_e in the SOL.

Below the x-point, additional energy loss from flux tubes occurs by radial transport into the

private flux region (PFR). The effect is not as large as might be imagined considering that the private region has no source of energy, because magnetic flux expansion is large near the x-point, reducing the radial temperature gradient. For typical DIII-D divertor configurations, UEDGE predicts only about 10-12% of the outer-divertor SOL power diffuses into the PFR, and reducing χ_e nearly to zero in the private region reduces this fraction to just less than 10%, with a corresponding rise in peak heat flux of less than 20%.

V. Relationship between midplane temperature profiles and divertor heat-flux profiles

The large uncertainties in the divertor heat flux database for ITER, as well as projections of very high heat flux for DEMO, have motivated increased interest in quantifying the dependence of the divertor heat flux profile width on core plasma parameters and upstream/midplane SOL temperature profiles [7]. Figure 3 shows that the full $1/e$ width of the outer divertor heat flux profile, when mapped back to the midplane, is nearly a factor of two larger than the electron temperature e-folding length $\lambda_{q,mid}/\lambda_{T,mid} = 0.6$, as compared to 2/7=0.28). Here we have computed the slope of the temperature profile over the range 0 to 0.4 cm just outside the separatrix, in the region where the divertor heat flux peaks and begins to fall off. As shown, the ratio $\lambda_{q,mid}/\lambda_{T,mid}$ is relatively insensitive to χ_e.

Moving beyond comparisons with 1D conduction, we have also examined the parameter dependence of the divertor heat flux profile width as predicted from the 2-point SOL model. Using the output from the full set of UEDGE parameter scans to determine $n_{e,sep}$, $T_{e,sep}$, and $\lambda_{q,mid}$, we evaluated the two-point model results (Sec. II) to obtain $\lambda_{q,mid} \equiv \lambda_{q,2\text{point}}$ for comparison. Midplane separatrix values for n_e and T_e were taken from UEDGE. As shown in Fig. 4, where we plot normalized $\lambda_{q,2\text{point}}$ vs $\lambda_{q,mid}$ from UEDGE, the conduction-limited two-

point model reproduces the full 2D solution reasonably well. Note that, to account for the detailed geometrical factors missing from the two-point model, all $\lambda_{q,2\text{point}}$ values have been normalized by a single constant factor to match the UEDGE value at $\lambda_{q,mid} = 0.256$ cm. Note that, for $\lambda_{q,mid} \le 0.4$ cm, the ratio of $T_{e,mid}$ to $T_{e,div}$ falls below 2, suggesting that the SOL should transition from the conduction-limited to sheath limited regime; this transition is much more evident when comparing UEDGE against Eq. (5), which is cannot be shown here due to space limitations.

VI. Effect of poloidally varying transport coefficients

It is widely recognized that assuming spatially uniform radial transport coefficients for particles and energy is likely an oversimplification for the scrape-off layer. Indeed, a radial variation in χ_e is often required to match simulation with experimental profiles in the SOL. It may be argued that SOL model validation will require a complete 2D map of the edge turbulence, but such measurements will not be available soon.

Here we explore how varying the poloidal distribution of the radial energy flux across the separatrix may affect both the divertor heat flux and midplane electron temperature profiles. We note that the larger surface area and compression of the outboard flux surfaces due to the Shafranov shift will peak radial transport at the outboard midplane significantly even with spatially uniform D and χ [2]. Giving the transport coefficients a ballooning character ($\chi \propto 1/\mathrm{B}^2$ or even $1/\mathrm{B}^3$) will lead to additional peaking of the radial transport at the outboard midplane $\left(B_T \propto 1/R\right)$. In all cases considered, the radial energy flow ($\mathrm{W/m^2}$) is peaked at the outboard midplane $\left(\theta = 270°\right)$, with half the total power coming out within a full-width at half-maximum varying from $\pm 50°$ (uniform $\chi = 0.5$ $\mathrm{m^2/s}$) to $\pm 40°$ ($\chi \propto 1/\mathrm{B}^3, 0.18 \le \chi \le 1.5$ m_2 /s).

Increasing the poloidal peaking of the radial transport acts in the same manner as reducing a spatially uniform transport coefficient. In effect, radial transport is relatively lower everywhere except in one section of the SOL, and lower χ leads to a narrower heat flux profile. Thus, if data is only available at midplane and divertor locations, it appears extremely hard to see any measurable difference in basic SOL properties resulting from poloidally non-uniform transport coefficients. Fig. 5 compares computed midplane electron temperature profiles and divertor heat flux profiles for two cases having nearly the same field-line average $\chi_{ave} = (1/L_{||}) \int \chi(\ell) d\ell_{||}$ but very different form for χ: 81bb has uniform D, $\chi = 0.5\ \mathrm{m}^2/\mathrm{s}$ and ii has $\chi \propto 1/\mathrm{B}^3$ with $\chi_{ave} = 0.49\ \mathrm{m}^2/\mathrm{s}$. The differences between the profiles are smaller than variations in typical DIII-D data; though not shown, the same holds true for divertor n_e and T_e profiles.

VII. Conclusions

This work reemphasizes that physics validation of the tokamak scrape-off layer physics requires application of comprehensive 2D analysis tools to make quantitative comparisons between midplane and divertor parameters. Using midplane ("upstream") temperatures near the separatrix or temperature scale length coupled with 1D or "2-point" models to predict the peak divertor heat flux and profile widths can introduce significant systematic error unless the models are calibrated by a full 2D calculation. Further uncertainties will almost certainly arise when impurity transport, detachment physics, and particle drifts are added to the problem. For quantities of interest such as the divertor heat or particle flux, parameter variations and cross-tokamak comparisons should focus on these quantities, mapped back to the midplane to account for topological considerations, rather than introducing additional complexity by relating data via secondary quantities.

The weak dependence of divertor heat flux and midplane temperature profiles on the poloidal variation of radial transport coefficients suggests that validating SOL models by aiming for ever more comprehensive diagnostic coverage around the boundary may be of limited value. On the other hand, the robustness of the basic scaling obtained from the simple 2-point model should motivate increased emphasis on parameter variations to validate the physics of the scrape-off layer. The value of using 2D simulation tools to explore the physics of the scrape-off layer and to identify and motivate new diagnostics and experiments cannot be overemphasized.

Acknowledgment

This work was supported by the U.S. Department of Energy under DE-FC02-04ER54698 and DE-AC52-07NA27344.

References

[1]. T.D. Rognlien, *et al*., Contrib. Plasma Phys. **34**, (1994) 362, and T. Rognlien, *et al*., J. Nucl. Mater. **196-198** (1992) 347.

[2] Gary .D. Porter, *et al*., Phys. Plasmas **3** (1996) 1967-1975.

[3] G.D. Porter, *et al*., Phys. Plasmas, **7** (2000), 3663-3690.

[4] G.D. Porter, *et al*., Fusion Sci. Technol. **48** (2005) 1127-1140.

[5] C.S. Pitcher, *et al,*, Plasma. Phys. Control. Fusion **39** (1997) 779-930.

[6] P. Stangeby, The Plasma Boundary of Magnetic Fusion Devices, Institute of Physics Publishing, Bristol and Philadelphia, 2000.

[7] R. Goldston, Phys. Plasmas **17**, (2010) 012503.

Figure Captions

Fig. 1. Poloidal distribution of parallel and perpendicular heat flux into the SOL as a function of parallel length along a field line 1.7 mm outside separatrix: blue - parallel heat flux $q_{\|}$ (◆ solid) on 1.7 mm field line, radial heat flux $q_{\perp}$ across separatrix (○ dashed) and $T_e/25$ (red-solid). Inboard midplane is at L=28.8 m.

Fig. 2. Outer-leg divertor heat flux profiles from UEDGE (red solid), Eq. (3) (■ blue solid), and their ratio (green dashed).

Fig. 3. Midplane scale lengths for electron temperature, λT_e, divertor heat flux, λQ, and value predicted from 2-point model (0.28 λT_e).

Fig. 4. Comparison between equivalent midplane heat flux profile as determined from conduction limited 2-point model [Eq. (5)] and 50 UEDGE divertor heat flux calculations mapped to midplane. Normalization for 2-point model data as indicated by arrow at y = 0.216).

Fig. 5. Comparison of midplane electron temperature profiles and outer divertor heat flux profiles for case ii: uniform $\chi = 0.5$ m^2/s and case bb: $\chi \propto 1/\mathrm{B}^3$ with $\chi_{ave} = 0.49$ m^2/s.

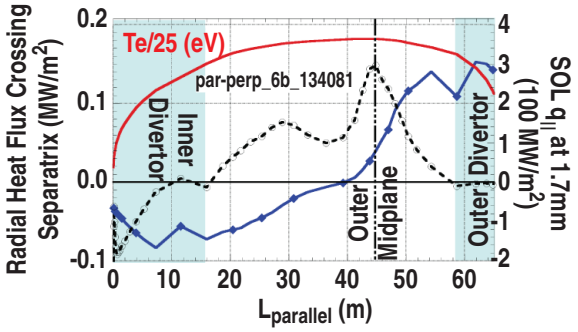

Figure 1, revised

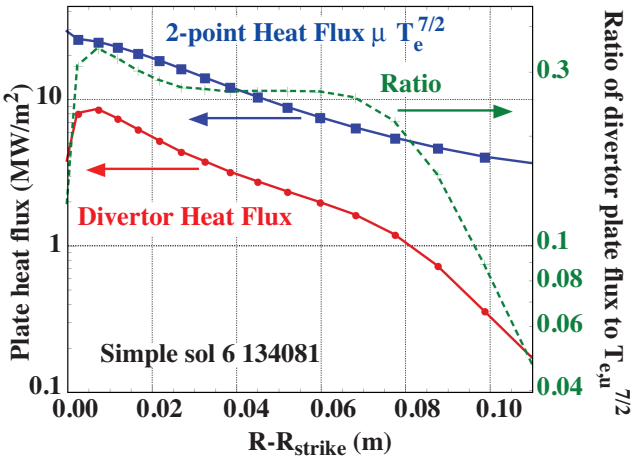
2-point Heat Flux μ T_e^7/2
Ratio
Divertor Heat Flux
Simple sol 6 134081
Plate heat flux (MW/m^2)
Ratio of divertor plate flux to T_e,u^7/2
R-R_strike (m)
10
1
0.1
0.3
0.1
0.08
0.06
0.04
0.00
0.02
0.04
0.06
0.08
0.10

Figure 2

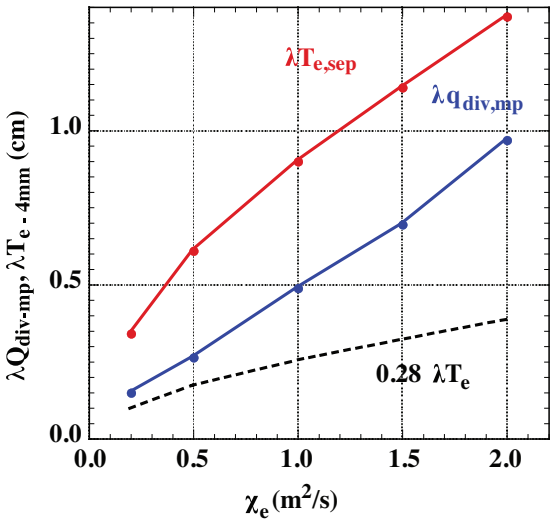
λT_e,sep
λq_div,mp
0.28 λT_e
λQ_div-mp, λT_e - 4mm (cm)
χ_e (m²/s)
0.0
0.5
1.0
1.5
2.0
0.0
0.5
1.0

Figure 3

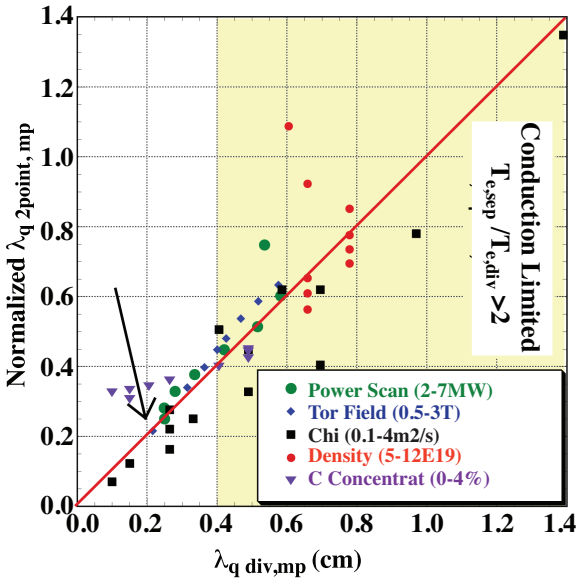
Normalized λq 2point, mp
λq div,mp (cm)
Conduction Limited
Te,sep /Te,div >2
Power Scan (2-7MW)
Tor Field (0.5-3T)
Chi (0.1-4m2/s)
Density (5-12E19)
C Concentrat (0-4%)
0.0
0.2
0.4
0.6
0.8
1.0
1.2
1.4

Figure 4

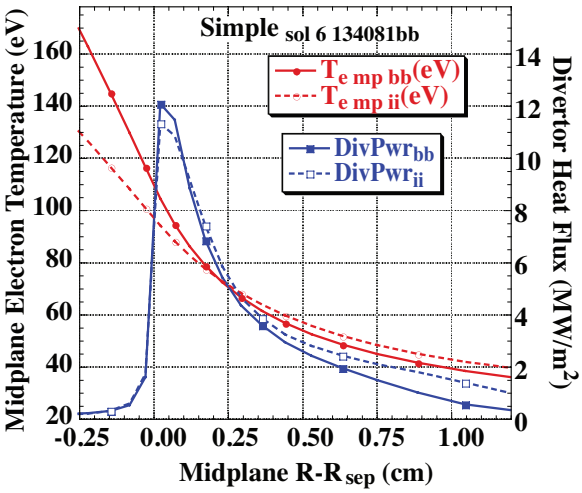
Simple sol 6 134081bb
Te mp bb(eV)
Te mp ii(eV)
DivPwrbb
DivPwrii
Midplane Electron Temperature (eV)
Divertor Heat Flux (MW/m2)
Midplane R-Rsep (cm)
160
140
120
100
80
60
40
20
14
12
10
8
6
4
2
0
-0.25
0.00
0.25
0.50
0.75
1.00

Figure 5

Attachment D
Scaling of divertor heat flux profile widths in DIII-D

C.J. Lasnier[1], M.A. Makowski[1], J.A. Boedo[2], N.H. Brooks[3], D.H. Hill[1], A.W. Leonard[3], and J.G. Watkins[4]

e-mail:Lasnier@LLNL.gov

[1]Lawrence Livermore National Laboratory, Livermore, California, USA
[2]University of California-San Diego, La Jolla, California, USA
[3]General Atomics, PO Box 85608, San Diego, California 92186-5608, USA
[4]Sandia National Laboratories, Albuquerque, New Mexico, USA

Abstract. Recent experiments in DIII-D have led to a new empirical scaling of divertor heat flux width $\lambda_{q,div}$ as a function of plasma parameters. Previous scaling efforts around the world have led to various scaling rules not all in agreement with each other. We controlled conditions during parameters scans as closely as possible to prevent other complicating variations. We varied B_T at constant I_p, I_p at constant B_T, and B_T/I_p at constant q_{95}. The neutral beam injected power was changed at constant I_p and B_T. Line-averaged density was varied at constant I_p and B_T. We find $\lambda_{q,div}$ is principally dependent on the plasma current to the -1.24 power. Our results agree with previous conduction-limited scalings from JET and NSTX, but exclude other scalings from both JET and other devices.

1. Introduction

The width of the divertor heat flux profile $\lambda_{q,div}$ is of great interest in future large tokamaks as well as many present devices. Previous studies examining the parametric dependence of $\lambda_{q,div}$ have arrived at diverse scalings [1] in JET [2], ASDEX-Upgrade [3], JT60-U [4,5], DIII-D [6,7], and NSTX [8]. With the aim of resolving this disagreement, we performed measurements in lower single-null edge localized mode (ELM)ing H-mode diverted configurations. We varied toroidal field (B_T) at constant plasma (I_p), I_p at constant B_T, and B_T/I_p at constant q_{95}. The neutral beam injected power P_{inj} was changed at constant I_p and B_T. Line-averaged density $\bar{n}_e$ was varied at constant I_p and B_T. The divertor heat flux was calculated from infrared camera measurements using a new high-resolution fast-framing IR camera.

The IR camera recorded divertor plate surface thermal emission at multi-kilohertz frame rates through the whole discharge, so that time-averaged data as well as rapid changes due to ELMs were obtained. The heat flux at each position in the radial profile was calculated at each of the times steps using the THEODOR 2D heat flux analysis code [9]. The THEODOR code has a capability of including a surface layer of arbitrary effective thickness to account for fast surface cooling often observed during transients. This layer must be chosen empirically using the surface temperature history. In order to make the simplest possible assumptions, no surface layer effects were assumed in the heat flux calculation. This results in some overshoot when the surface temperature falls after an ELM pulse. Consequently we avoid the time slices immediately after an ELM in this analysis.

In an effort to separate the physics of ELM heat flux scaling from the scaling of the inter-ELM heat flux, we chose time slices least affected by ELMs. Therefore

heat flux data was averaged from a time 20% into the inter-ELM interval until 95% of the way to the onset of the subsequent ELM, prior to exponential profile fitting. This fixed fraction of the ELM period was chosen so as to reduce the impact of overshoot in the heat flux calculation resulting from the previous ELM, due to the effect of surface layers mentioned above. The overshoot is most pronounced immediately after the ELM heat flux peak and then falls off with time.

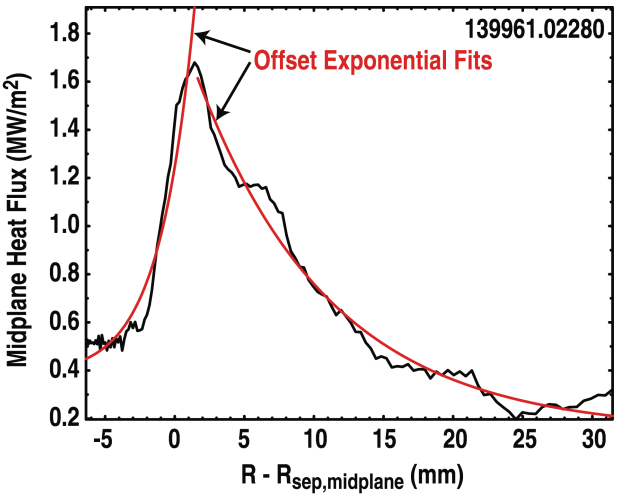

FIG. 1. Typical heat flux profile after mapping to the midplane as a function of distance from the separatrix at the midplane, R-$R_{sep,mp}$, showing offset exponential fits.

The heat flux profiles were coherently averaged for these inter-ELM times over multiple inter-ELM intervals of nearly fixed conditions.

The outer strike point heat flux profile was mapped to outer midplane and fitted on the public and private flux side with separate exponential ($a_0 + a_1 e^{x/\lambda}$) profiles (Fig. 1) [10]. The heat flux width $\lambda_{q,div,midplane}$ is taken to be the sum of the two exponential widths. This is different from the integral width proposed by Loarte [11], in which the integral of the profile is divided by the peak. Our heat flux profiles show plateau values in the private flux and far scrape-off-layer (SOL), at a level too large to be accounted for by absorbed radiation or plasma interaction. It is possible that there is some effect of internal optical reflections. The plateau effect is still being investigated. Due to these flat areas in the common and the private flux areas far from the separatrix, Loarte width would depend on the arbitrary width of the integration window, so is unsatisfactory measure here whereas sum of the exponential widths is not sensitive to this parameter.

We show scaling of the profile width as a function of the parameters varied, and compare with published results from other devices.

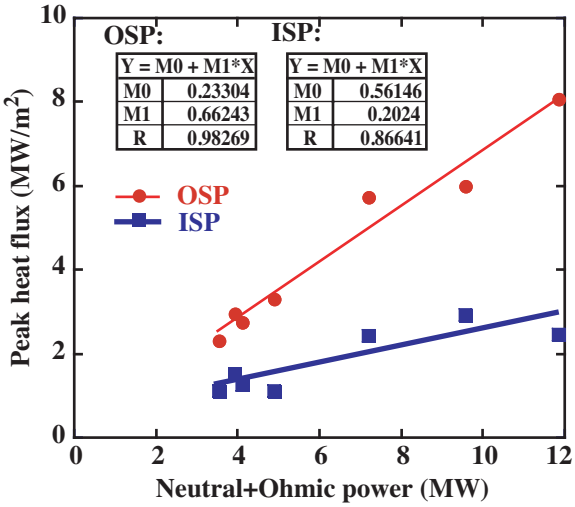

FIG. 2. Fig. 1: ELM-averaged peak heat flux at the ISP and OSP plotted against the input power. Linear fits to the data are plotted, with fitting parameters shown in the boxes. The dependence on input power

2. Variation in $\lambda_{q,div}$ with Plasma Parameters

Multi-parameter fits were made to investigate the scaling of $\lambda_{q,div}$ with I_p (plasma current), q_{95} (safety factor at the 95% flux surface), n_e (electron density), B_T (toroidal field), P_{SOL} [power flow into the SOL], P_{inj} (neutral beam injected power), s_{95} (magnetic shear at the 95% flux surface), and α_{95} (dimensionless pressure gradient at the 95% flux surface).

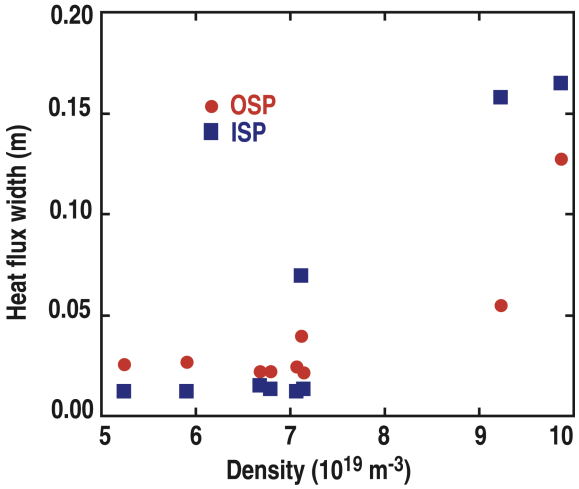

FIG. 3. Dependence of divertor heat flux profile width on density. There is essentially no effect below the detachment threshold.

We found both in the present analysis between ELMs and the previous analysis averaged over ELMs [12] only very weak dependence of $\lambda_{q,div}$ on total input power P_{in}, which in these discharges is the sum of P_{inj} and the Ohmic heating power.

We illustrate this in Fig. 2, where peak heat flux averaged over ELMs is plotted against input power. The peak heat flux increases linearly with input power. By conservation of energy, the heat flux profile width stays fixed. As found on NSTX, JET and ASDEX-Upgrade (DIVII), we find essentially no (or very weak) dependence of the width on input power.

In Fig. 3, for the case with averaging over ELMs [12], the full widths at half maximum (FWHM) of the heat flux in the divertor are shown plotted against line-averaged density. The FWHM is used here because the heat flux profiles at higher density are not well-fit by the exponentials defined above. At low density, $\lambda_{q,div}$ is independent of $\bar{n}_e$, but there is a threshold density of ~7x10^{19} m^{-3} where the profile becomes wider, representing the onset of detachment. In the density scan from which this data was extracted, P_{in} was 4.9–5.1 MW, except for the densities $\bar{n}_e = 5.2\times10^{19}$ m^{-3} and $\bar{n}_e = 6.8\times10^{19}$ m^{-3} where $P_{in} = 7.2$ MW, and $P_{in} = 4.1$ MW, respectively. Since we found

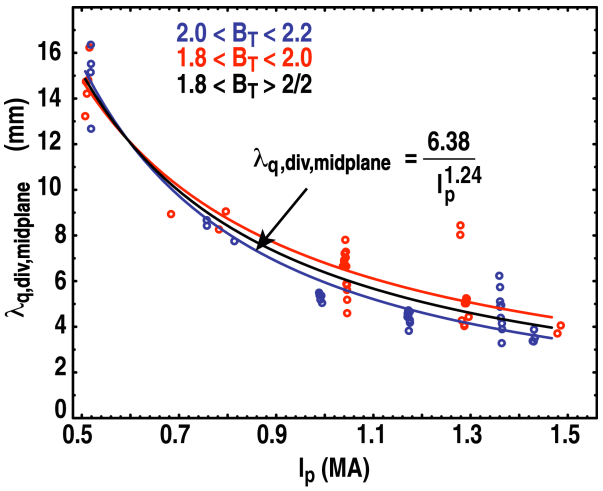

FIG. 4. Dependence of heat flux width (mapped to the midplane) on plasma current. The red, black, and blue symbols denote various ranges of toroidal field, showing little effect from changing B_T.

$\lambda_{q,div}$ does not depend on input power, this power variation does not affect the widths obtained from the density scan at these densities. Toroidal field was held constant at B_T = -1.9 T, and plasma current was held at I_p = 1.3 MA.

The effect of radiation from the outboard divertor on the strike point heat flux profile is small for the low-density attached discharges. It becomes significant at the onset of detachment where we see the profile broadening, and in fully detached strike points not considered here, the radiated power absorbed by the divertor plate accounts for nearly all the measured heat flux.

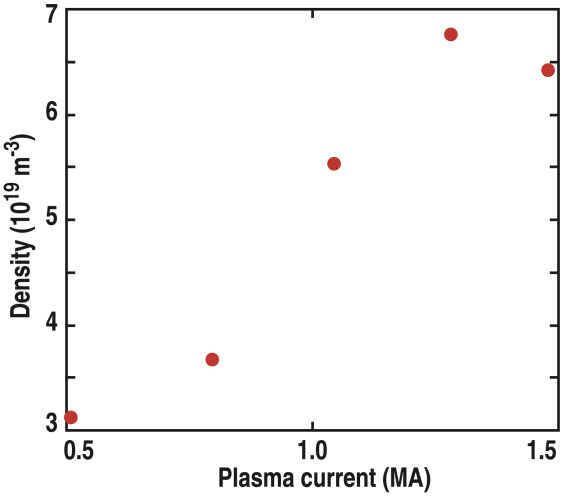

FIG. 5. Variation of line-averaged electron density during the plasma current scan. All these densities are at the low end of Fig. 2, so there was little effect of the density variations on the heat flux width.

We find that $\lambda_{q,div,midplane}$ is larger at low plasma current, as shown in Fig. 4 [10], where $\lambda_{q,div,midplane}$ is plotted against I_p. The width decreases inversely as a power of the plasma current close to unity, namely $\lambda_{q,div,midplane} = 6.38/I_p^{1.24}$. Similar behavior is seen in NSTX [8] where the width decreases with increasing plasma current, approximately as $1/I_p$.

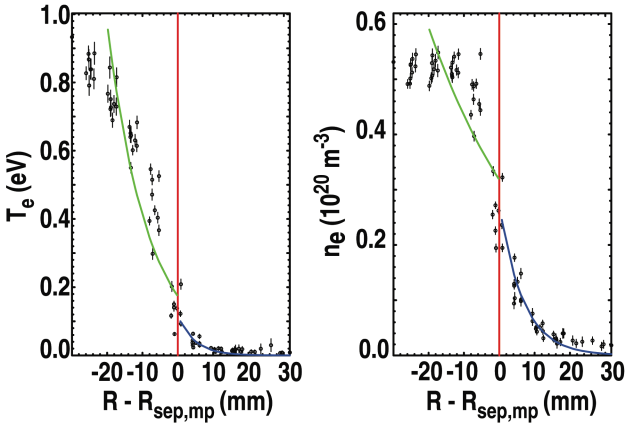

FIG. 6. Typical outer midplane electron temperature and density profiles mapped from Thomson scattering measurements to the outer midplane. The curves show the exponential fits.

We know that core plasma confinement improves at higher plasma current [13], and the behaviour observed is consistent with cross-field SOL transport also being reduced as plasma current increases. For this scan of plasma current, toroidal field was held fixed at B_T = -1.9 T, and P_{inj} = 4.7–5.0 MW, except for the point at I_p = 1.3 MA where P_{inj} = 4.1 MW. Density was not held constant, but allowed to vary at the natural H-mode density, because of practical difficulty measuring the heat flux at the OSP during the plasma pumping that would have been required to maintain constant density. Figure 5 [12] shows the line-averaged density variation during the I_p scan. Note that the range of densities is within the zone of Fig. 3 where the density variation shows little effect on the heat flux width. Also, the density remains at low Greenwald fraction as I_p is raised and consequently the detachment threshold is raised along with the density. Therefore the density variation during the I_p scan does not affect the heat flux width.

For the inter-ELM data, the widths $\lambda_{q,div,midplane}$ showed no discernable trend in the multi-parameter fits with toroidal field B_T, in contrast to the case where the data was averaged over ELMs [12]. We varied B_T from 1.2 to 2.1 T (ion ∇B drift toward the lower divertor). No correlation was seen between $\lambda_{q,div}$ and B_T. The dependence on plasma current but not toroidal field is not fully understood.

3. Divertor Heat Flux Profile Width in Relation to Upstream Temperature

Figure 6 [10] shows typical T_e (electron temperature) and n_e (electron density) profiles at the outer midplane derived from Thomson scattering measurements in the upper outer SOL. Typically 10–20 profiles were coherently averaged over a 200 ms window, from time slices just before ELMs. The Thomson profile data were mapped along field lines to the outer midplane. For each parameter (n_e and T_e) exponential fits were made to the data near the separatrix, from inside and outside, which gave the electron temperature gradient scale lengths, λ_{Te}^{int} and λ_{Te}^{SOL}, respectively. The λ_{Te}^{SOL} was found to have less scatter than either the λ_{Te}^{int} or a hyperbolic tangent fit width. The fitted λ_{Te}^{SOL} is not sensitive to the method of determining the separatrix location. The divertor heat flux profile widths $\lambda_{q,div,midplane}$ were compared with upstream λ_{Te}^{SOL}, showing a very weak correlation (Fig. 7) [10]. This is contrary to two-point models that give that predict $\lambda_{Te} = (7/2)\lambda_q$ [14].

We can conclude that the heat flux profiles for the most part are wider than predicted by the two-point model. Departures from that model are to be expected due to the presence of radial transport, radiation within the transport volume, and recycling in the divertor, which these two-point models neglect.

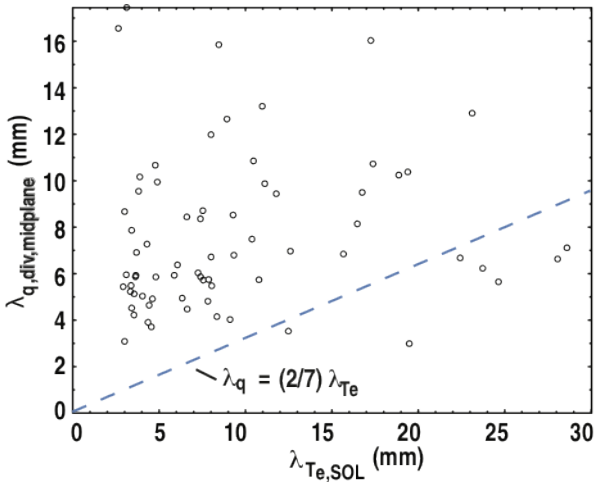

FIG. 7. Plot of the heat flux width, $\lambda_{q,div,midplane}$, versus the Thomson electron temperature profile e-folding length in the scrape off layer, λ_{Te}^{SOL}. The widths are larger than expected from a two point model, $\lambda_q = (2/7)\lambda_{Te}$, which is shown by the blue dashed line.

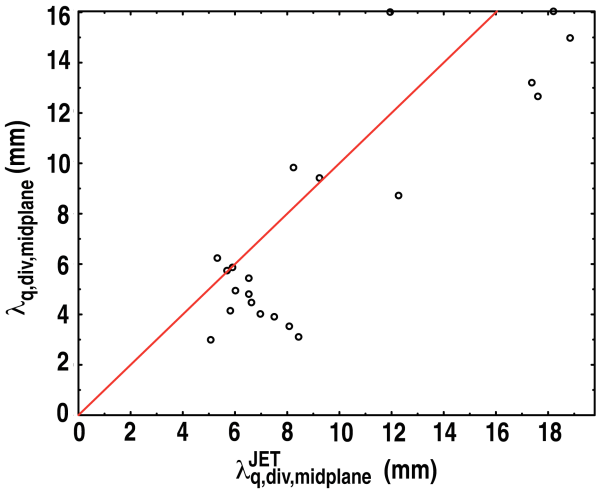

FIG. 8. Comparison of DIII-D heat flux profile width with the JET conduction-limited scaling applied to the same DIII-D data. The red line has a slope of unity. The DIII-D results are in reasonable agreement with the JET scaling.

4. Comparison with Other Scaling Results

The results of the present scaling study are in rough agreement with the JET scaling of conduction limited heat flux widths [15], given by

$$\lambda_{q,miplane}^{JET}\,(\mathrm{mm}) = 2.41\times10^{-5}\; B_T^{-1}(\mathrm{T})\; P_{SOL}^{-1/2}\,(\mathrm{MW})\; n_e^{1/4}\left(\mathrm{m}^{-3}\right) q_{95}R^2\,(\mathrm{m}) \quad . \qquad (1)$$

The comparison between the present DIII-D scaling and Eq. (1) is shown in Fig. 8 [10]. The dominant dependence is in $q_{95}/B_T \sim 1/I_p$. The density dependence is weak in the JET scaling law, in agreement with our observations. However, our fits show no dependence on P_{SOL}, the power crossing the separatrix. With no machine size variation in our data to compare with the R^2 dependence from JET, we are left with $1/I_p$ from Eq. (1), which is similar to our finding. Our finding of no dependence of the width on input power is in direct contrast to Eq. (1).

The heat flux width prediction from Ref. [5] was also considered:

$$\lambda_{q,midplane}^{H\text{-}2}\,(\mathrm{mm}) = 5.3P^{0.38}\,(\mathrm{MW})\; B_T^{-0.71}(\mathrm{T})\;\; q_{95}^{0.3} \quad . \qquad (2)$$

The widths predicted by Eq. (2) are 10 times smaller than those found in DIII-D [10]. Equation (2) contains no scaling for machine size.

5. Comparison of Divertor Heat Flux Profiles with UEDGE Modeling

Modeling of discharges from the plasma current scan using the UEDGE code [16] has been initiated, in an attempt to identify what physical mechanism causes the heat flux width to change with plasma current. The power flow through the SOL, and the midplane electron temperature and density profiles are taken from the experimental data. However, there is sufficient scatter in the experimental electron temperature and density data that widely varying profiles could be chosen that are all within the error bars. Transport coefficients in UEDGE are adjusted until the upstream profiles agree with the experiment. In the results reported here, best agreement with the heat flux width was obtained when drifts were turned on at 20% of full value, and poor agreement when drifts were turned off. The comparison between the experimentally determined heat flux profile and the UEDGE output for I_p = 1.5 MA, the highest plasma current reached in the I_p scan, is shown in Fig. 9 [10] as a function of poloidal distance along the horizontal divertor surface. The experimental data are much lower than the UEDGE prediction, and the data are multiplied by a factor of 5.2 in the plot to match the UEDGE prediction at its peak value. The uncertainty in the upstream profiles creates a large margin of error in the UEDGE predictions of divertor heat flux and other divertor parameters. In addition, it is possible in the experiment to have heat deposited in unobserved locations whereas UEDGE, to achieve power balance, places that heat at the outer strike point. Further work is needed to reconcile these differences.

The measured radiated power was 350 kW. This value was approximately matched in UEDGE (300 kW) when the flows were turned on at 20%, but the code greatly underestimated the radiated power (90 kW) when drifts were turned off. The heat flux profile in the model was narrower than in the experiment. Some degree of shoulder in seen in both the measured and experimental profile.

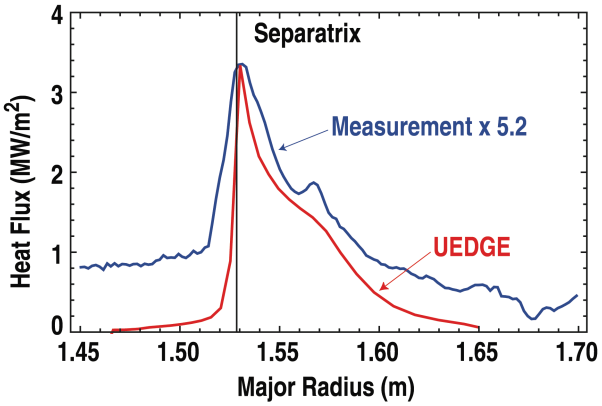

FIG. 9. Comparison of measured heat flux (blue, multiplied by 5.2) and that predicted by UEDGE (blue) [10]. For this case I_p =1.5 MA.

These preliminary attempts at UEDGE modeling are the beginning of a more in-depth effort to compare these measurements with modeling and to aid in understanding the physical origin of the scaling with plasma current. It is clear that drifts are important in interpreting the result, but we must obtain agreement with experimental data with drifts fully turned on.

6. Conclusion

In DIII-D, we find the strongest dependence of the divertor heat flux profile width is on the plasma current. The heat flux width varies inversely as the 1.24 power of the plasma current and not at all with input power. Our result is in substantial agreement with the conduction-limited JET scaling of Ref. [15] for plasma current but not for power, but not at all with the multi-machine scaling of Ref. [5]. We are not able to confirm any dependence of the heat flux width on the near-separatrix SOL fall-off length of the outer midplane temperature profile, although we find the simple two-point models do not provide an adequate description of the heat flux transport. Our heat flux profiles are substantially wider than predicted by the two-point model. We find no evidence in the multi-parameter fitting of a significant dependence on B_T or P_{SOL}. The lack of change in heat flux profile width in spite of the change in field line connection length with B_T indicates reduction in cross-field SOL transport with B_T. The physical mechanism leading to the scaling of λ_q with I_p is not yet understood, but we note that increasing I_p is known to reduce radial transport inside the separatrix and we suspect a similar effect in the SOL. Attempts to compare the data with the UEDGE modeling code have begun, and we find that drifts are important in matching the heat flux profile width. At this point we still see substantial differences between the model and experiment. Further modeling will be done to help understand the I_p dependence of the heat flux profile.

This work was supported by the US Department of Energy under DE-AC52-07NA27344, DE-FG002-07ER4917, DE-FC02-04ER54698, and DE-AC04-94AL85000.

References

[1] LOARTE, A., *et al.,* Nucl Fusion **47** (2007) S203
[2] EICH, T., *et al.,* J. Nucl. Mater. **333-339** (2005) 669
[3] HERRMANN, A., Plasma Phys. Control. Fusion **44** (2002) 883
[4] ITER Physics Basis Editors, Nucl. Fusion **39** (1999) 2137
[5] LOARTE, A., *et al.,* J. Nucl. Mater. **266-269** (1999) 587
[6] HILL, D.N., *et al.,* J. Nucl. Mater **196-198** (1992) 204
[7] LASNIER, C.J., *et al.,* Nucl. Fusion **38** (1998) 1225
[8] MAINGI, R., *et al.,* J. Nucl. Mater **363-365** (2007) 196
[9] HERRMANN, A., *et al.*, Plasma Phys. Control. Fusion **37** (1995) 17
[10] MAKOWSKI, M.A., *et al.,* "Comparison of Upstream *T*e Profiles with Downstream Heat Flux Profiles and Their Implications on Parallel Heat Transport in the SOL in DIII-D," Proc. of 19th International Conference on Plasma-Surface Interactions, San Diego, CA, 2010 and submitted for publication in J. Nucl. Mater.
[11] LOARTE, A., *et al.*, J. Nucl. Mater. **266-269** (1999) 587
[12] LASNIER, C.J., *et al.*, Proc. of 36th EPS Conference on Plasma Phys., Sofia, 2009 ECA Vol. 33E, P-4.140
[13] J.G. Cordoy and ITER Confinement Database and Modelling Working Group, Plasma Phys. Control. Fusion **39** (1997) B115–B127
[14] PITCHER, C.S. AND STANGEBY, P.C., Plasma Phys. Control. Fusion **39** (1997) 779
[15] KIRNEV, G., *et al.*, Plasma Phys. Control. Fusion **49** (2007) 689
[16] ROGNLIEN, T., *et al.,* J. Nucl. Mater. **196-198** (1992) 347